

CONSISTENCY OF BLOCKING TRANSFORMATIONS IN THE FINITE-TEMPERATURE RENORMALIZATION GROUP

Sen-Ben Liao^{1,2†} and Michael Strickland^{3‡}

*Department of Physics*¹
National Chung-Cheng University
Chia-Yi, Taiwan R. O. C.

*Laboratory of Theoretical Physics*²
Louis Pasteur University
3 rue de l'Université 67087 Strasbourg, Cedex, France

and

*Department of Physics*³
Ohio State University
Columbus, Ohio 43210 U.S.A.

Submitted to *Nucl. Phys. B*

ABSTRACT

The finite-temperature renormalization group is formulated via the Wilson-Kadanoff blocking transformation. Momentum modes and the Matsubara frequencies are coupled by constraints from a smearing function which plays the role of an infrared cutoff regulator. Using the scalar $\lambda\phi^4$ theory as an example, we consider four general types of smearing functions and show that, to zeroth-order in the derivative expansion, they yield qualitatively the same temperature dependence of the running constants and the same critical exponents within numerical accuracy.

CCU-TH-98-01

March 1998

[†] electronic address: senben@phy.ccu.edu.tw

[‡] electronic address: strickland.41@osu.edu

I. INTRODUCTION

Finite-temperature renormalization group (RG) techniques provide a powerful means of probing the physical behavior of a quantum system interacting with an external heat bath. The presence of the additional length scale $\beta = T^{-1}$, the inverse of the temperature, makes the theory more complicated since there are now two types of fluctuations, quantum and thermal, which compete with one another. In order to apply the RG framework to explore issues such as the QCD deconfinement phase transition and the evolution of the early universe, one must first understand the subtle interplay between these fluctuations.

To take into account both thermal and quantum fluctuations, various finite-temperature RG prescriptions have been proposed [1], [2]. These RG schemes also provide an improvement beyond perturbative approximations, which are known to be plagued by infrared (IR) singularities in the high-temperature limit as well as in the vicinity of criticality. In the present work, we revisit the studies of Ref. [1] which were based on the Wilson-Kadanoff blocking transformation [3] performed on a manifold $S^1 \times R^d$ in the imaginary-time formalism. By introducing a regulating smearing function $\rho_{\tilde{n},k}^{(d)}(\mathbf{x}, \tau_x)$, which simulates the coarse graining in momentum space, the effective degrees of freedom of the theory are now characterized by the blocked fields, $\phi_{\tilde{n},k}$,

$$\phi_{\tilde{n},k}(\mathbf{x}, \tau_x) \equiv \int_0^\beta d\tau_y \int_{\mathbf{y}} \rho_{\tilde{n},k}^{(d)}(\mathbf{x} - \mathbf{y}, \tau_x - \tau_y) \phi(\mathbf{y}, \tau_y), \quad (1.1)$$

where $\phi(x)$ represents the original field variables. While \tilde{n} is a discrete cutoff for the Matsubara frequencies $\omega_n = 2\pi n/\beta$, the scale k may be regarded as a generalized IR cutoff for a combination of both $|\mathbf{p}|$ and ω_n . Varying k infinitesimally then allows us to generate a nonlinear differential RG equation for the blocked action $\tilde{S}_{\beta,k}[\Phi]$, which is defined by

$$e^{-\tilde{S}_{\beta,k}[\Phi(\mathbf{x})]} = \int_{\text{periodic}} D[\phi] \prod_{\mathbf{x}} \delta(\phi_k(\mathbf{x}) - \Phi(\mathbf{x})) e^{-S[\phi]}. \quad (1.2)$$

The blocked action provides a smooth interpolation between the bare action $S_\Lambda[\Phi]$ and the quantum effective action which generates the one-particle-irreducible graphs as k is lowered from the ultraviolet (UV) cutoff, Λ , to zero. We have taken the field average of a given block $\Phi(\mathbf{x})$ to coincide with the slowly varying background. Since the flow equation for $\tilde{S}_{\beta,k}[\Phi]$ is too complicated to be solved exactly, we make an expansion in powers of derivatives:

$$\tilde{S}_{\beta,k}[\Phi] = \int_0^\beta d\tau \int_{\mathbf{x}} \left\{ \frac{Z_{\beta,k}(\Phi)}{2} (\partial_\tau \Phi)^2 + \frac{Z_{\beta,k}(\Phi)}{2} (\nabla \Phi)^2 + U_{\beta,k}(\Phi) + O(\partial^4) \right\}. \quad (1.3)$$

The theory is then parameterized by a set of coupled nonlinear partial differential RG equations for the wavefunction renormalization constant, $Z_{\beta,k}(\Phi)$, the blocked potential, $U_{\beta,k}(\Phi)$ and higher-order contributions. The behavior of the theory at any arbitrary k and T can then be studied by analytically or numerically solving these coupled equations. We shall designate this type of RG prescription as the momentum RG, or MRG.

Notice that the functional form of $\rho_{\tilde{n},k}^{(d)}(\mathbf{x}, \tau_x)$ in MRG is not unique; different choices will change the way in which the irrelevant, short-distance degrees of freedom are eliminated in course of blocking. In the finite-temperature setting, how the two types of modes, ω_n in S^1 and $|\mathbf{p}|$ in R^d , are block averaged is controlled by $\rho_{\tilde{n},k}^{(d)}(\mathbf{x}, \tau_x)$. In Fourier space, $\rho_{\tilde{n},k}^{(d)}(\mathbf{p}, \omega_n)$ modifies the bare propagator as

$$\frac{1}{\mathbf{p}^2 + \omega_n^2 + \mu_R^2} \longrightarrow \frac{\rho_{\tilde{n},k}^{(d)}(\mathbf{p}, \omega_n)}{\mathbf{p}^2 + \omega_n^2 + \mu_R^2}. \quad (1.4)$$

Thus, one may visualize the following possibilities: (i) Blocking is performed in only one of the two subspaces, i.e., with $\rho_{\tilde{n}}(\tau_x)$, or $\rho_k^{(d)}(\mathbf{x})$; (ii) both ω_n and $|\mathbf{p}|$ are blocked, but with two smearing functions $\rho_{\tilde{n}}(\tau_x)$ and $\rho_k^{(d)}(\mathbf{x})$ that are independent of one another; and (iii) a constraint exists in the smearing function for ω_n and $|\mathbf{p}|$ which allows them to be coupled and eliminated in some coherent manner. The trivial case of no blocking simply implies the absence of any RG transformation. Scenario (iii) is the most interesting case because it allows us to examine the interplay between the quantum and thermal fluctuations in the two spaces. In this paper smearing functions corresponding to the above categories are constructed explicitly. In particular, we study, in Fourier space, $\rho_k^{(d)}(\mathbf{p}) = \Theta(k - |\mathbf{p}|)$ for category (i), $\rho_{\tilde{n},k}^{(d)}(\mathbf{p}, \omega_n) = \Theta(k - |\mathbf{p}|)\Theta(\tilde{n} - |n|)$ for (ii), and $\rho_k^{(d)}(\mathbf{p}, \omega_n) = \Theta(k - \sqrt{\omega_n^2 + |\mathbf{p}|^2})$ and $\rho_k^{(d)}(\mathbf{p}, \omega_n) = \Theta(k - |\omega_n| - |\mathbf{p}|)$ for (iii). These smearing functions differ only in their treatment of the coupling between $|\mathbf{p}|$ and the $n \neq 0$ sector. Thus, by comparing the numerical solutions of the corresponding RG equations, one can gain insight into the importance of the feedback between ω_n and $|\mathbf{p}|$.

To derive the MRG equations, we lower k infinitesimally from k to $k - \Delta k$, where Δk is the characteristic thickness of the RG shell that contains the modes to be eliminated. The ratio $\kappa = \Delta k/k$ represents the fraction of the modes that are eliminated in each blocking step. When the smearing function involves n explicitly, the resulting RG becomes piecewise continuous due to the discreteness in the Matsubara frequencies. However, we shall find that in all the cases considered, qualitatively the same results are obtained for the temperature dependence of the running parameters. The quantitative difference stems from the boundary conditions on the RG flow when the Matsubara modes are blocked.

We also show that all four methods yield the same critical exponents to within 0.5% when $U_{\beta,k}(\Phi)$ is expanded in a power series in Φ near criticality. Thus, it may be concluded that the feedbacks between $|\mathbf{p}|$ and the $n \neq 0$ sector can be treated perturbatively in the high T regime. Although scaling patterns in the IR regime differ in all four cases, direct correspondence may nevertheless be established and equivalence may be recovered in some cases.

We emphasize that κ must always remain small in order to trace out the true RG evolution. A large κ causes poor tracking of the RG trajectory. To illustrate this point, we examine the high-temperature behavior of the quartic coupling constant of the scalar $\lambda\phi^4$ theory in the symmetric phase. It has been shown that $\lambda_\beta = \lambda_{\beta,k=0}$ decreases with increasing T but approaches a constant using $\rho_k^{(d)}(\mathbf{p}) = \Theta(k - |\mathbf{p}|)$ [4]. However, if one employs the ‘‘Matsubara shell assumption’’ with $\Delta k = 2\pi/\beta$, i.e., the thickness of the RG

shell is chosen to be equal to the spacing between two adjacent Matsubara frequencies, an incorrect high-temperature behavior will be obtained. The result is due to the fact that as Δk becomes increasing large in the high T limit, κ is no longer small and the flow then deviates significantly from its true trajectory.

The organization of the paper is as follows: In Sec. II we give four examples of the MRG smearing functions and describe the details of how the corresponding RG evolution equations are generated. We compare and contrast the manner in which ω_n and $|\mathbf{p}|$ are coupled. Numerical solutions for the MRG equations are presented in Sec. III. We demonstrate once more how $\lambda_{\beta,k=0}$ decreases with increasing T and may be approximated by a constant in the infinite-temperature limit. Results extracted from the Matsubara shell assumption are also included to illustrate its failure in the high-temperature limit. Sec. IV is reserved for summary and discussions. In Appendix A we present a complementary RG scheme, the temperature RG (TRG), which is formulated using T as the running parameter. Its consistency with MRG is demonstrated. In Appendix B the connection between the finite-temperature behavior of the running parameters and the fixed points is established. In particular, we identify all the fixed points accessible by both the MRG and the TRG schemes and show that the existence of an infinite-temperature Gaussian fixed point rules out the possibility of $\lambda_{\beta,k=0}$ increasing with T .

II. MRG SMEARING FUNCTIONS

As described in the Introduction, under blocking transformations an IR cutoff k is introduced into the theory by defining the coarse-grained fields (1.1) via a smearing function $\rho_{\tilde{n},k}^{(d)}(\mathbf{x}, \tau_x)$. Here \tilde{n} differentiates between the high and the low Matsubara frequencies, and k provides a separation between the slowly varying background fields and the fast-fluctuating modes which are to be integrated over. Below we consider four smearing functions, each of which has a different coupling between ω_n and $|\mathbf{p}|$.

(1) $\rho_k^{(d)}(\mathbf{p}) = \Theta(k - |\mathbf{p}|)$:

The simplest blocking is to choose a sharp cutoff in the R^d submanifold, leaving S^1 unconstrained. In position space, this smearing function has the form

$$\rho_k^{(d)}(\mathbf{x}) = \int_{|\mathbf{p}| < k} e^{i\mathbf{p} \cdot \mathbf{x}}, \quad (2.1)$$

which approaches $\delta^d(\mathbf{x})$ as $k \rightarrow \infty$. This limit corresponds to a completely “unblocked” bare system characterized by the original unrenormalized fields. The blocked fields take on the form [4]

$$\phi_k(\mathbf{x}, \tau_x) = \int_{\mathbf{y}} \rho_k^{(d)}(\mathbf{x} - \mathbf{y}) \phi(\mathbf{y}, \tau_x) = \frac{1}{\beta} \sum_{n=-\infty}^{\infty} \int_{|\mathbf{p}| < k} e^{-i(\omega_n \tau_x - \mathbf{p} \cdot \mathbf{x})} \phi_n(\mathbf{p}). \quad (2.2)$$

We see that the effect of this smearing is to provide an integration over $|\mathbf{p}| > k$ for all n . However, with this choice of $\rho_k^{(d)}(\mathbf{x})$, no averaging is done in the τ_x direction.

Let us first consider the simple, independent-mode approximation where all the modes greater than k are eliminated at once with no feedback being taken into account. The perturbative one-loop correction to the blocked potential reads:

$$\begin{aligned}\tilde{U}_{\beta,k}^{(1)}(\Phi) &= \frac{1}{2\beta} \sum_{n=-\infty}^{\infty} \int'_{\mathbf{p}} \ln[\omega_n^2 + \mathbf{p}^2 + V''(\Phi)] = \frac{1}{\beta} \int'_{\mathbf{p}} \ln \sinh\left(\frac{\beta\sqrt{\mathbf{p}^2 + V''(\Phi)}}{2}\right) \\ &= \frac{1}{2\beta} \int'_{\mathbf{p}} \left\{ \beta\sqrt{\mathbf{p}^2 + V''(\Phi)} + 2 \ln[1 - e^{-\beta\sqrt{\mathbf{p}^2 + V''(\Phi)}}] \right\} + \dots,\end{aligned}\quad (2.3)$$

where the prime notation in the integration implies $k < |\mathbf{p}| < \Lambda$. The wavefunction renormalization constant has been set to unity for simplicity. A direct differentiation of the above expression with respect to k then gives

$$k \frac{d\tilde{U}_{\beta,k}(\Phi)}{dk} = -\frac{S_d k^d}{2\beta} \left\{ \beta\sqrt{k^2 + V''(\Phi)} + 2 \ln[1 - e^{-\beta\sqrt{k^2 + V''(\Phi)}}] \right\}, \quad (2.4)$$

where $S_d = 2/(4\pi)^{d/2}\Gamma(d/2)$. Unfortunately the equation has a serious drawback in that it only accounts for the one-loop contribution and neglects the important feedback from the higher to the lower modes whose energy scales, in principle, may differ by several orders of magnitude. Since the effective degrees of freedom of the theory are not well tracked, it will fail to capture the relevant physics in the high temperature limit as well as in the neighborhood of the phase transitions.

The aim of MRG is precisely to take into consideration the important higher loop corrections and the couplings between the modes. In Figure 1 we depict how RG is carried out as an improvement beyond the independent-mode approximation. At $k = \Lambda$, the system is unblocked and no modes are eliminated. As the system undergoes blocking with the IR cutoff being lowered from k to $k - \Delta k$, the modes contained inside the RG shell of thickness Δk are integrated out. The elimination of these fast-fluctuating modes results in a more complicated blocked potential $U_{\beta,k-\Delta k}(\Phi)$ which contains more operators than the previous one, $U_{\beta,k}(\Phi)$. The evolution is complete when k finally reaches zero. By lowering k infinitesimally, the RG equation reads:

$$k \frac{dU_{\beta,k}(\Phi)}{dk} = -\frac{S_d k^d}{2\beta} \sum_{n=-\infty}^{\infty} \ln[\omega_n^2 + k^2 + U''_{\beta,k}(\Phi)], \quad (2.5)$$

which, upon summing over n , yields

$$k \frac{dU_{\beta,k}(\Phi)}{dk} = -\frac{S_d k^d}{2\beta} \left\{ \beta\sqrt{k^2 + U''_{\beta,k}(\Phi)} + 2 \ln[1 - e^{-\beta\sqrt{k^2 + U''_{\beta,k}(\Phi)}}] \right\}. \quad (2.6)$$

The functional forms of Eqs. (2.4) and (2.6) are remarkably similar, except for the substitution on the right-hand-side of the latter by the scale-dependent counterpart, i.e.,

$V''(\Phi) \rightarrow U''_{\beta,k}(\Phi)$. Though this “dressing” seems straight-forward, it has been demonstrated to have far-reaching consequences, particularly in the study of phase transitions and critical phenomena. By solving the equations numerically subject to the initial condition $U_{\beta=\infty,\Lambda}(\Phi) = V_\Lambda(\Phi)$, where $V_\Lambda(\Phi)$ is the bare potential defined at the UV cutoff Λ , the severe IR divergences encountered in the finite-loop calculations are completely removed. In addition, critical exponents can be measured to a remarkable precision through numerical solutions of the exact renormalization group flow equations [5].

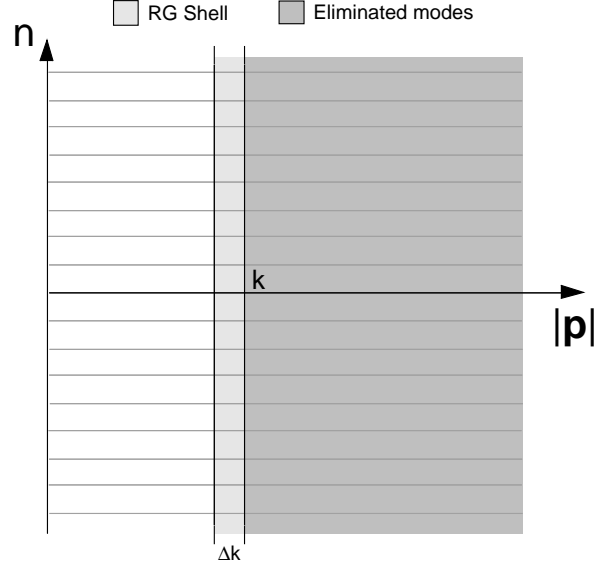


Figure 1. Schematic diagram of blocking Method 1.

It is useful to compare Eq. (2.6) with the zero-temperature result for D dimensions, obtained using a sharp cutoff for D -dimensional momentum integration [6]:

$$k \frac{dU_k(\Phi)}{dk} = -\frac{S_D k^D}{2} \ln[k^2 + U''_k(\Phi)]. \quad (2.7)$$

In the regime where $\bar{\beta} \rightarrow 0$, the contribution from the first term in (2.6) can be neglected and one has

$$k \frac{dU_{\beta,k}(\Phi)}{dk} = -\frac{S_d k^d}{2\bar{\beta}} \ln[k^2 + U''_{\beta,k}(\Phi)], \quad (2.8)$$

which is simply the contribution from the $n = 0$ mode, as can be seen from (2.5). Thus, we see clearly that the $n = 0$ sector alone is sufficient to account for the d -dimensional characteristics. Upon rescaling of $\Phi \rightarrow \beta^{-1/2}\Phi$ and $U_{\beta,k} \rightarrow \beta^{-1}U_k$, Eq. (2.8) coincides with Eq. (2.7) for $D = d$.

On the other hand, in the low T regime where $\bar{\beta} \rightarrow \infty$ (holding k fixed), a complete summation over n is necessary for recovering the proper zero-temperature $(d+1)$ -dimensional feature of the theory. The expected RG equation is that of Eq. (2.7) with $D = d+1$. However, in this limit Eq. (2.6) gives

$$k \frac{dU_k(\Phi)}{dk} = -\frac{S_d k^d}{2} \sqrt{k^2 + U''_k(\Phi)} \quad (2.9)$$

instead. A careful comparison of the RG flow governed by Eqs. (2.7) and (2.9) shows that they lead to the same renormalized values for the vertex functions at $k = 0$, but differ in the scalings patterns for $k \ll \mu_R$, where μ_R is the renormalized mass of the theory [4]. How can we improve our RG to ensure that the desirable IR scaling limits below the mass gap are attained? To do so, one must carefully take into account the couplings between ω_n and $|\mathbf{p}|$. From Figure 1, it is clear that Method 1 results in a complete summation over all Matsubara modes within a given RG shell and ignores the couplings between modes having the same $|\mathbf{p}|$ but with different n 's. How do we take into consideration this coupling, and how important is this to physical applications? To answer these questions, we must examine other smearing functions.

$$(2) \quad \rho_{\tilde{n},k}^{(d)}(\mathbf{p}, \omega_n) = \Theta(k - |\mathbf{p}|) \Theta(\tilde{n} - |n|):$$

As an improvement to account for the systematic feedback between certain d -dimensional momentum modes $|\mathbf{p}|$ and the Matsubara frequencies ω_n , we choose the smearing function to be $\rho_{\tilde{n},k}^{(d)}(\mathbf{p}, \omega_n) = \Theta(k - |\mathbf{p}|) \Theta(\tilde{n} - |n|)$, or

$$\rho_{\tilde{n},k}^{(d)}(\mathbf{x}, \tau_x) = \rho_{\tilde{n}}(\tau_x) \rho_k^{(d)}(\mathbf{x}) = \frac{1}{\beta} \sum_{|n| < \tilde{n}} \int_{|\mathbf{p}| < k} e^{-i(\omega_n \tau_x - \mathbf{p} \cdot \mathbf{x})}, \quad (2.10)$$

which implies:

$$\phi_k(\mathbf{x}, \tau_x) = \frac{1}{\beta} \sum_{|n| < \tilde{n}} \int_{|\mathbf{p}| < k} e^{-i(\omega_n \tau_x - \mathbf{p} \cdot \mathbf{x})} \phi_n(\mathbf{p}). \quad (2.11)$$

In other words, this smearing function provides a summation over $n > |\tilde{n}|$ in S^1 and an integration over all $|\mathbf{p}| > k$ in R^d . From

$$\delta(\tau_x) = \frac{1}{\beta} \sum_{n=-\infty}^{\infty} e^{-i\omega_n \tau_x}, \quad (2.12)$$

one can readily verify again that the limits $k \rightarrow \Lambda$ and $\tilde{n} \rightarrow \infty$ correspond to $\rho_{\tilde{n},k}^{(d)}(\mathbf{x}, \tau_x) \rightarrow \delta^d(\mathbf{x})\delta(\tau_x)$ and the theory coincides with the original “unblocked” system. With such a step-by-step elimination, the couplings between different Matsubara frequencies are also taken into account [7].

It turns out that the bounds on n can actually be chosen in a more physically motivated manner. To do so, we notice that just as the high modes with $|\mathbf{p}| > k$ in R^d are being integrated over, we should also sum over in S^1 all the high Matsubara frequencies with $|\omega_n| > k$, or $|n| > [\bar{\beta}/2\pi]$, where $\bar{\beta} = \beta k$ and $[j]$ is the greatest integer less or equal to j . A similar upper bound, $\beta\Lambda/2\pi$ on ω_n , or equivalently, $n_{\max} = [\beta\Lambda/2\pi]$ may also be imposed. The blocking procedure of this scheme is depicted in Figure 2.

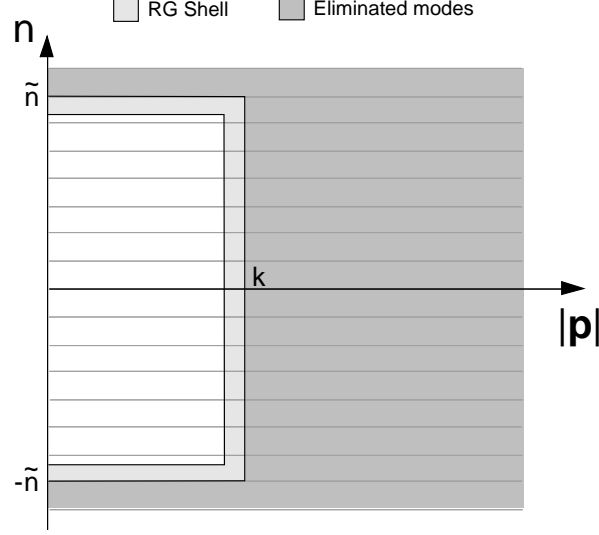


Figure 2. Schematic diagram of blocking Method 2. The thickness of the RG shell in the n -axis is zero for $\Delta k \rightarrow 0$ (exaggerated here), but a Matsubara mode is eliminated after \mathcal{N} continuous iterations where $[\mathcal{N}\beta\Delta k/2\pi]=1$.

From the figure, we see that the RG shell on the $\omega_n - |\mathbf{p}|$ plane can be subdivided into three parts: one vertical strip having a thickness Δk containing modes with $|n| \leq [\bar{\beta}/2\pi]$, and two horizontal strips with $|\mathbf{p}| < k$. In the limit $\Delta k \rightarrow 0$, the contribution from the two horizontal strips vanishes, as long as Δk does not span a Matsubara mode. It is crucial not to make the Matsubara shell assumption with $\Delta k = 2\pi/\beta$ such that all three volumes contribute. Such an assumption will lead to serious difficulties, particularly in the high temperature regime where Δk becomes so large that the treatment would be reduced to that of the independent-mode approximation. Thus, one always makes Δk small to ensure that the RG shell contains as few modes as possible. The subtraction of a Matsubara mode takes place only after every \mathcal{N} continuous iterations of RG in the $|\mathbf{p}|$ space when $\mathcal{N}\Delta k = 2\pi/\beta$ and the condition $[\mathcal{N}\beta\Delta k/2\pi] = 1$ is reached. Similar blocking iterations are then repeated until we arrive at $n = 0$.

The above prescription leads to

$$\begin{aligned}
 U_{\beta,k-\Delta k} - U_{\beta,k} &= \frac{1}{2\beta} \sum_{|n| \leq [\frac{\bar{\beta}}{2\pi}]} \int_{\mathbf{p}} \Theta(|\mathbf{p}| - k + \Delta k) \Theta(k - |\mathbf{p}|) \ln \left[\omega_n^2 + p^2 + U''_{\beta,k}(\Phi) \right] \\
 &= \frac{S_d}{2\beta} \sum_{n=-[\frac{\bar{\beta}}{2\pi}]}^{[\frac{\bar{\beta}}{2\pi}]} \int_{k-\Delta k}^k dp p^{d-1} \ln \left[\omega_n^2 + p^2 + U''_{\beta,k}(\Phi) \right],
 \end{aligned} \tag{2.13}$$

or, in the limit $\Delta k \rightarrow 0$,

$$k \frac{dU_{\beta,k}(\Phi)}{dk} = -\frac{S_d k^d}{2\beta} \sum_{n=-[\bar{\beta}/2\pi]}^{[\bar{\beta}/2\pi]} \ln \left[\omega_n^2 + k^2 + U''_{\beta,k}(\Phi) \right]. \tag{2.14}$$

We see that contrary to Eq. (2.6) in Method 1, the summation over n is now restricted to that contained in the shell, namely $|n| \leq [\bar{\beta}/2\pi]$. This RG coincides with Eq. (2.8) as $\bar{\beta} \rightarrow 0$. On the other hand, when $\bar{\beta} \rightarrow \infty$, one recovers (2.5) or (2.6) which contains both zero and finite-temperature sectors for $d+1$ dimensions. However, the latter contributes only perturbatively [5].

The situation becomes slightly more complicated when one arrives at the step where a particular mode along the n -axis, say $\pm\omega_m$ ($n = \pm m$), is contained in Δk and is to be eliminated. In this case, the RG equation becomes

$$\begin{aligned}
U_{\beta,k-\Delta k}(\Phi) - U_{\beta,k}(\Phi) &= \frac{1}{2\beta} \sum_{n=-\infty}^{\infty} \int_{\mathbf{p}} \left\{ \Theta(|\mathbf{p}| - k + \Delta k) \Theta(|n| < [\frac{\bar{\beta}}{2\pi}]) + \delta_{n,\pm m} \right\} \\
&\quad \times \Theta(k - |\mathbf{p}|) \ln \left[\omega_n^2 + p^2 + U''_{\beta,k}(\Phi) \right] \\
&= \frac{S_d k^{d-1}}{2\beta} (\Delta k) \sum_{|n| \leq [\frac{\bar{\beta}}{2\pi}] - 1} \ln \left[\omega_n^2 + p^2 + U''_{\beta,k}(\Phi) \right] \\
&\quad + \frac{S_d}{\beta} \int_0^k dp p^{d-1} \ln \left[\omega_m^2 + p^2 + U''_{\beta,k}(\Phi) \right],
\end{aligned} \tag{2.15}$$

where the last term represents the contribution from $\pm\omega_m$. For $d=3$ we can evaluate the last term analytically

$$\begin{aligned}
&\frac{1}{2\pi^2} \int_0^k dp p^2 \ln \left[\omega_m^2 + p^2 + U''_{\beta,k}(\Phi) \right] \\
&= \frac{1}{6\pi^2} \left\{ k^3 \ln \left[k^2 + \omega_m^2 + U''_{\beta,k} \right] + 2 \left[\omega_m^2 + U''_{\beta,k} \right]^{3/2} \tan^{-1} \left(\frac{k}{\sqrt{\omega_m^2 + U''_{\beta,k}}} \right) \right. \\
&\quad \left. + 2k \left[\omega_m^2 + U''_{\beta,k}(\Phi) \right] \right\}.
\end{aligned} \tag{2.16}$$

The absence of the Δk factor in the expression prevents us from generating a differential equation for $U_{\beta,k}(\Phi)$. Nevertheless, Eq. (2.15) can be solved numerically.

$$(3) \quad \rho_k^{(d)}(\mathbf{p}, \omega_n) = \Theta(k - \sqrt{\omega_n^2 + |\mathbf{p}|^2}):$$

The above smearing function represents another class of finite-temperature blocking, and has been considered in Refs. [8] and [9]. In position space, it corresponds to

$$\rho_k^{(d)}(\mathbf{x}, \tau_x) = \frac{1}{\beta} \sum_{n=-\infty}^{\infty} \int_{\mathbf{p}} e^{-i(\omega_n \tau_x - \mathbf{p} \cdot \mathbf{x})} \Theta(k - \sqrt{\omega_n^2 + |\mathbf{p}|^2}). \tag{2.17}$$

This particular choice of $\rho_k^{(d)}(\mathbf{p}, \omega_n)$ leads to a mixing between the components in the subspaces S^1 and R^d , and the Matsubara sum over n is now constrained by the value of

k , similar to Method 2 but in a more complicated manner. Figure 3 depicts how modes contained in the RG shell are eliminated as k is lowered.

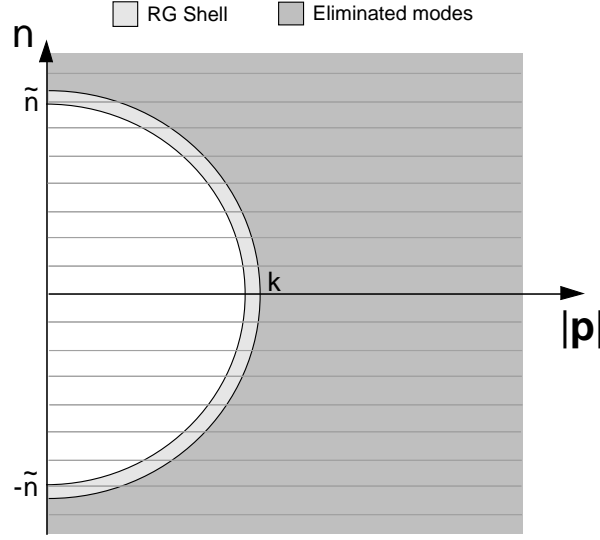


Figure 3. Schematic diagram of blocking Method 3.

If the RG shell does not contain a Matsubara mode along the n -axis, a nonlinear differential flow equation can be obtained as

$$\begin{aligned}
k \frac{dU_{\beta,k}(\Phi)}{dk} &= -\frac{k}{2\beta} \sum_{n=-\infty}^{\infty} \int_{\mathbf{p}} \ln \left[\omega_n^2 + \mathbf{p}^2 + U''_{\beta,k}(\Phi) \right] \delta(\sqrt{\omega_n^2 + |\mathbf{p}|^2} - k) \\
&= -\frac{S_d k^2}{2\beta} \sum_n' \int_0^{\infty} dp \frac{p^{d-1}}{\sqrt{k^2 - \omega_n^2}} \ln \left[\omega_n^2 + p^2 + U''_{\beta,k}(\Phi) \right] \delta(p - \sqrt{k^2 - \omega_n^2}) \\
&= -\frac{S_d k^2}{2\beta} \ln \left[k^2 + U''_{\beta,k}(\Phi) \right] \sum_n' (k^2 - \omega_n^2)^{\frac{d-2}{2}} \\
&= -\frac{S_d k^d}{2\beta} g^{(d)}(\bar{\beta}) \ln \left[k^2 + U''_{\beta,k}(\Phi) \right],
\end{aligned} \tag{2.18}$$

where

$$g^{(d)}(\bar{\beta}) = 1 + 2 \sum_{n=1}^{[\bar{\beta}/2\pi]} \left[1 - \left(\frac{2\pi n}{\bar{\beta}} \right)^2 \right]^{\frac{d-2}{2}}, \tag{2.19}$$

is a piece-wise continuous function of $\bar{\beta}$, as depicted in Figure 4 for $d = 3$.

On the other hand, as in Method 2, an additional contribution representing the $|m|$ -th Matsubara mode along the n -axis appears during their elimination, and the equation

reads:

$$\begin{aligned}
U_{\beta,k-\Delta k}(\Phi) - U_{\beta,k}(\Phi) &= \frac{1}{2\beta} \sum_{n=-\infty}^{\infty} \int_{\mathbf{p}} \Theta(k - \sqrt{\omega_n^2 + |\mathbf{p}|^2}) \left\{ \Theta(\sqrt{\omega_n^2 + |\mathbf{p}|^2} - k + \Delta k) \right. \\
&\quad \left. + \delta_{n,\pm m} \Theta(\sqrt{\omega_n^2 + |\mathbf{p}|^2} - \omega_m) \right\} \ln \left[\omega_n^2 + p^2 + U''_{\beta,k}(\Phi) \right] \\
&= \frac{S_d k^{d-1}}{2\beta} (\Delta k) \tilde{g}^{(d)}(\bar{\beta}) \ln \left[k^2 + U''_{\beta,k}(\Phi) \right] \\
&\quad + \frac{S_d}{\beta} \int_0^{\sqrt{k^2 - \omega_m^2}} dp p^{d-1} \ln \left[\omega_m^2 + p^2 + U''_{\beta,k}(\Phi) \right],
\end{aligned} \tag{2.20}$$

where $\tilde{g}^{(d)}(\bar{\beta})$ is the same as $g^{(d)}(\bar{\beta})$ in (2.19) except the $n = \pm[\bar{\beta}/2\pi]$ contribution is excluded in the summation. Thus, we apply Eq. (2.20) whenever a particular $|\omega_m|$ is contained in the RG shell. It could happen that the modes lie exactly at the boundary of the shell, i.e., $k - \Delta k = \omega_m$. In this case one may easily verify that Eq. (2.20) reduces to Eq. (2.18) and a differential flow equation is recovered. Although one could in principle fine tune Δk with respect to T in a way such that the points along the n -axis always lie on the boundary of the shells, we shall treat Δk and T as independent input parameters.

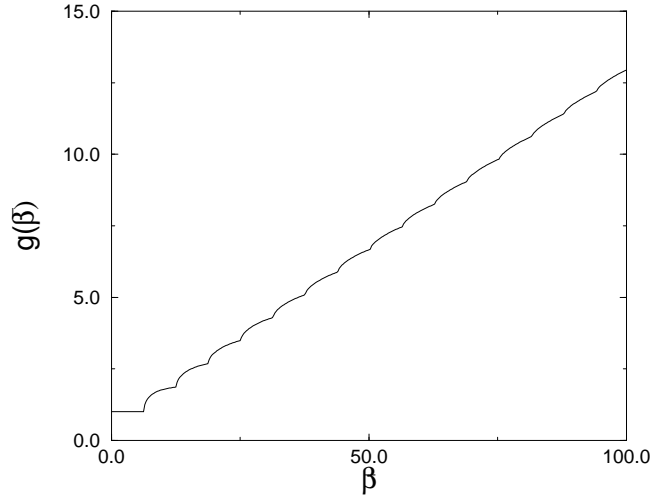


Figure 4. Plot of $g^{(3)}(\bar{\beta})$ for Method 3.

The novel feature of employing this type of blocking is that for both $\bar{\beta} \gg 1$ and $\bar{\beta} \ll 1$, one will obtain the expected zero-temperature result as given in Eq. (2.7), namely, $D = d + 1$ for $\bar{\beta} \gg 1$ and $D = d$ for $\bar{\beta} \ll 1$. This can be readily seen by noting that in the high-temperature limit $\bar{\beta} \rightarrow 0$ (decreasing β while holding k fixed), $g^{(d)}(\bar{\beta}) \rightarrow 1$ and Eq. (2.18) is reduced to Eq. (2.8). On the other hand, in the regime where $\bar{\beta} \gg 1$, the

summation in Eq. (2.19) can be replaced by an integral:

$$\begin{aligned}
g^{(d)}(\bar{\beta}) &\approx 1 + 2 \int_1^{\frac{\bar{\beta}}{2\pi}} dn \left[1 - \left(\frac{2\pi n}{\bar{\beta}} \right)^2 \right]^{\frac{d-2}{2}} \\
&= 1 + \sqrt{\pi} \frac{\Gamma(\frac{d}{2})}{\Gamma(\frac{d+1}{2})} \left(\frac{\bar{\beta}}{2\pi} \right) - 2F\left(\frac{1}{2}, 1 - \frac{d}{2}, \frac{3}{2}; \frac{4\pi^2}{\bar{\beta}^2}\right) = \frac{S_{d+1}}{S_d} \bar{\beta} + \dots.
\end{aligned} \tag{2.21}$$

In this limit, $S^1 \times R^d$ is effectively R^{d+1} and the RG equation is reduced to that of (2.7) with $D = d + 1$.

$$(4) \quad \rho_k^{(d)}(\mathbf{p}, \omega_n) = \Theta(k - |\omega_n| - |\mathbf{p}|):$$

The above smearing function represents yet another method of blocking at finite temperature. The manner in which the modes are eliminated is illustrated in Figure 5.

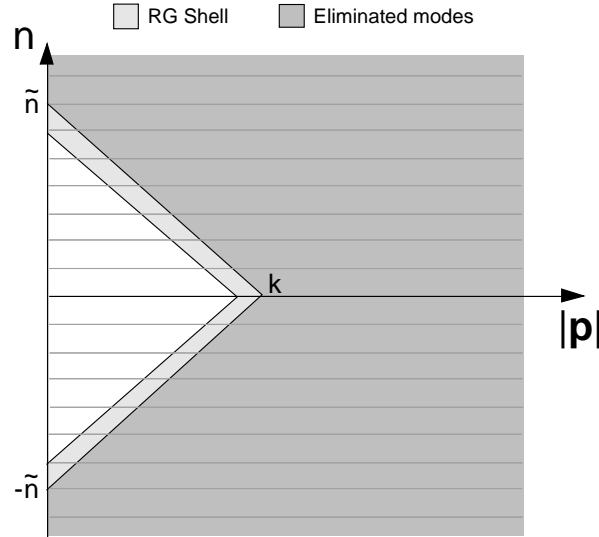


Figure 5. Schematic diagram of blocking Method 4.

In analogy to Method 3, the components $|\mathbf{p}|$ and ω_n are also mixed due to the constraint from the blocking function. By comparing the results obtained from these two schemes, one can gain insight into the effects of this mixing. The RG equations can be written as

$$\begin{aligned}
k \frac{dU_{\beta,k}(\Phi)}{dk} &= -\frac{k}{2\beta} \sum_{n=-\infty}^{\infty} \int_{\mathbf{p}} \ln \left[\omega_n^2 + \mathbf{p}^2 + U''_{\beta,k}(\Phi) \right] \left\{ \theta(n) \delta(\omega_n + |\mathbf{p}| - k) \right. \\
&\quad \left. + \delta_{n,0} \delta(|\mathbf{p}| - k) + \theta(-n) \delta(-\omega_n + |\mathbf{p}| - k) \right\} \\
&= -\frac{S_d k^d}{2\beta} \left\{ 2 \sum_{n=1}^{[\bar{\beta}/2\pi]} \left(1 - \frac{2\pi n}{\bar{\beta}} \right)^{d-1} \ln \left[\omega_n^2 + (k - \omega_n)^2 + U''_{\beta,k}(\Phi) \right] + \ln \left[k^2 + U''_{\beta,k}(\Phi) \right] \right\},
\end{aligned} \tag{2.22}$$

and

$$k \left(\frac{U_{\beta, k-\Delta k} - U_{\beta, k}}{\Delta k} \right) = \frac{S_d k^d}{2\beta} \left\{ 2 \sum_{n=1}^{[\bar{\beta}/2\pi]-1} \left(1 - \frac{2\pi n}{\bar{\beta}} \right)^{d-1} \ln \left[\omega_n^2 + (k - \omega_n)^2 + U''_{\beta, k}(\Phi) \right] \right. \\ \left. + \ln \left[k^2 + U''_{\beta, k}(\Phi) \right] \right\} + \frac{S_d k}{\beta(\Delta k)} \int_0^{k-\omega_m} dp p^{d-1} \ln \left[\omega_m^2 + p^2 + U''_{\beta, k}(\Phi) \right], \quad (2.23)$$

for an RG shell with and without a Matsubara frequency mode $|\omega_m|$ along the n -axis, respectively. Once more, Eqs (2.23) and (2.22) coincide when the mode lies exactly along the boundary with $k - \Delta k = \omega_m$.

For $\bar{\beta} \rightarrow 0$, Eq. (2.8) is again easily recovered. Similarly, for $\bar{\beta} \rightarrow \infty$, ω_n can be regarded as a continuous variable and we replace the summation by an integral. Dropping the subscript β in the potential, we obtain

$$k \frac{dU_k(\Phi)}{dk} = -\frac{S_d k^d}{2\beta} \left\{ \frac{\beta}{\pi} \int_{2\pi/\beta}^k d\omega_n \left(1 - \frac{\omega_n}{k} \right)^{d-1} \ln \left[\omega_n^2 + (k - \omega_n)^2 + U''_k(\Phi) \right] \right. \\ \left. + \ln \left[k^2 + U''_k(\Phi) \right] \right\} \\ = -\frac{S_d k^{d+1}}{2\pi} \int_{2\pi/\beta}^1 dx (1-x)^{d-1} \ln \left[x^2 + (1-x)^2 + \frac{U''_k(\Phi)}{k^2} \right] + \dots \quad (2.24) \\ \approx -\frac{S_d k^{d+1}}{2\pi} \ln \left[1 + \frac{U''_k(\Phi)}{k^2} \right] \int_0^1 dx (1-x)^{d-1} + \dots \\ = -\frac{S_d k^{d+1}}{2d\pi} \ln \left[1 + \frac{U''_k(\Phi)}{k^2} \right] + \dots$$

In going from the second to the third equation above, we have taken the limit $2\pi/\bar{\beta} \rightarrow 0$. In addition, since the argument in the logarithm does not change appreciably with x over the interval, we have dropped its x dependence and moved the expression outside the integral. While the expected logarithmic form of the RG flow is regained, the equation contains a factor $S_d/d\pi$ instead of the expected S_{d+1} for $D = d+1$ from Eq. (2.7). Such a constant overall mismatch, however, is harmless and can be eliminated by a simple rescaling: $k \rightarrow c^{1/(2-d)}k$ and $U_k(\Phi) \rightarrow c^{2/(2-d)}U_k(\Phi)$ with $c = S_d/S_{d+1}d\pi$ for $d \neq 2$.

Up to now we have discussed four types of smearing functions for setting up the finite-temperature MRG. In the limit $\bar{\beta} \rightarrow 0$, all four MRG equations reproduce the expected dimensionally reduced result. The agreement can be easily understood from the fact that at any arbitrary IR scale k , each of the four different RG shells always contains the static $n = 0$ mode which gives the dominant contribution for small $\bar{\beta}$, or the high-temperature limit. The $n \neq 0$ modes are strongly suppressed and can be treated perturbatively. In this regard, we expect to obtain qualitatively the same physical information from any of the four RG equations in the small $\bar{\beta}$ limit. We shall substantiate this claim later with numerical solutions.

On the other hand, the asymptotic forms of the four MRG equations in the large $\bar{\beta}$ regime all differ from one another. In Figure 6 the comparison between Methods 1 and 3 is depicted. The difference may be attributed to their treatment of couplings between $|\mathbf{p}|$ and the $\omega_{n \neq 0}$ modes. While the $n = 0$ sector alone has been shown to be sufficient to attain proper scalings for $\bar{\beta} \ll 1$, to reproduce the less trivial scalings in the $\bar{\beta} \gg 1$ regime will require a subtle and an intricate account of the feedbacks between $|\mathbf{p}|$ and these non-static modes. The analyses above show that only Method 3 is constructed in such a way that it leads to the desired low-temperature scalings for the running parameters, while rescalings or adjustments of the UV cutoff are required for the other methods.

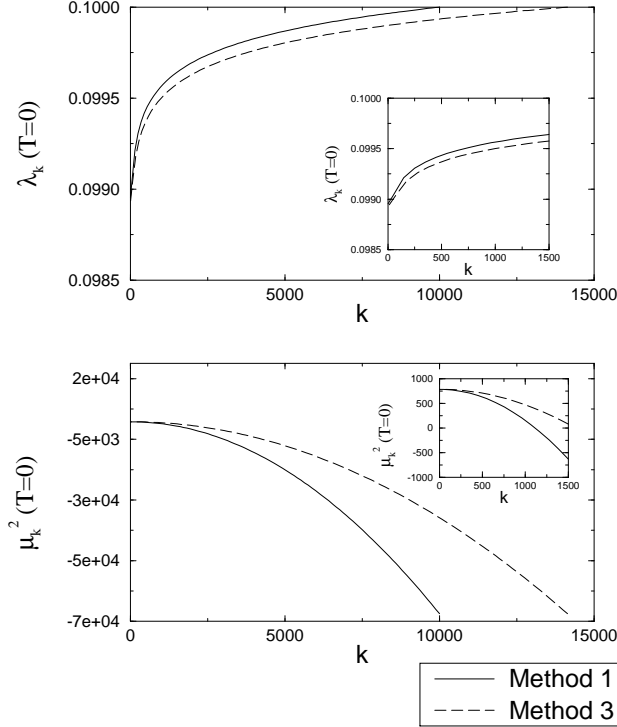


Figure 6. Zero-temperature RG flow using Methods 1 and 3. The figure shows that as long as the correction to the UV cutoff is taken into account both methods give the same renormalized couplings at $T=0$.

In passing we comment that there exists a complementary TRG in which β acts as the running parameter. When β is varied infinitesimally, the TRG leads to (see Appendix A)

$$\begin{aligned} \frac{\beta \partial U_{\beta,k}}{\partial \beta} = & - \int_{\mathbf{p}}' \left\{ \frac{1}{\beta} \ln \sinh \left(\frac{\beta}{2} \sqrt{\mathbf{p}^2 + U''_{\beta,\mathbf{p}}} \right) \right. \\ & \left. - \frac{1}{2} \left[\sqrt{\mathbf{p}^2 + U''_{\beta,\mathbf{p}}} + \beta \frac{\partial}{\partial \beta} \sqrt{\mathbf{p}^2 + U''_{\beta,\mathbf{p}}} \right] \coth \left(\frac{\beta}{2} \sqrt{\mathbf{p}^2 + U''_{\beta,\mathbf{p}}} \right) \right\}, \end{aligned} \quad (2.25)$$

with $k = \Lambda - \Delta k$ in the $|\mathbf{p}|$ integration. This equation is the finite-temperature analog of the renown Wegner-Houghton RG [10], and is consistent with the results obtained using

the MRG schemes. The general procedure of blocking transformation is not unique, and one can certainly construct other types of smearing functions in addition to what have been considered. There is an important stipulation, however, for what is considered to be an effective RG transformation – that it makes the smallest possible change in going from k to $k - \Delta k$ for any arbitrary k . In other words, the most successful scheme is the one whose RG shell contains the least number of modes. Only by doing so is the environment not altered grossly. In all four RG prescriptions, the fraction of the modes taken out from each blocking step is $\kappa = \Delta k/k$. Since each loop is accompanied by a power of κ , by taking this parameter to be infinitesimally small all higher loop corrections can be suppressed [10], [11]. This justifies our MRG equations, which are based on a simple one-loop framework. On the other hand, the failure of perturbation theory and the Matsubara shell assumption in the high-temperature regime can be readily explained by noting that $\kappa \approx 1$, which implies a dramatic change of the environment.

One could certainly consider a smearing function such as $\rho_{\tilde{n}}(\omega_n) = \Theta(\tilde{n} - |n|)$, where the RG evolution is now governed by a difference equation:

$$U_{\beta}^{\{\tilde{n}-1\}}(\Phi) = U_{\beta}^{\{\tilde{n}\}}(\Phi) + \frac{1}{\beta} \int_{\mathbf{p}} \ln \left[\omega_{\tilde{n}}^2 + \mathbf{p}^2 + U_{\beta}^{\{n\}''}(\Phi) \right], \quad (2.26)$$

or

$$U_{\beta}^{\{0\}}(\Phi) = U_{\beta}^{\{m\}}(\Phi) + \frac{1}{\beta} \sum_{n=1}^m \int_{\mathbf{p}} \ln \left[\omega_n^2 + \mathbf{p}^2 + U_{\beta}^{\{n\}''}(\Phi) \right]. \quad (2.27)$$

In this case eliminating $|\omega_m|$ implies taking away a fraction of modes, $\kappa' = 2/(2m+1)$, from the theory. However, κ' is clearly not small at all for small m . Hence this blocking method will break down in certain regimes.

III. NUMERICAL RESULTS

We now present the numerical results for the four MRG equations discussed in Sec. II. By expanding $U_{\beta,k}(\Phi)$ as a power series in Φ^2

$$U_{\beta,k}(\Phi) = \sum_{m=1}^{\infty} g_{\beta,k}^{(2m)} (\Phi^2)^m, \quad (3.1)$$

followed by a truncation at Φ^{14} , we transform the non-linear partial differential MRG equation into a set of non-linear coupled ordinary differential equations for the couplings, $\{g_{\beta,k}^{(2m)}\}$. These equations are then integrated using a fourth-order, adaptive step-size, Runge-Kutta integrator. We take $d = 3$ for definiteness.

As pointed out in Section II, an entirely continuous RG flow is not obtained when $|\mathbf{p}|$ and ω_n are coupled. In particular, the continuous RG flow equations in the form of differential equations, e.g. (2.13), can be employed only when the RG shell to be eliminated does not span a Matsubara mode. However, when a Matsubara mode, say $|\omega_m|$, is contained in the shell, a discrete, e.g. (2.15), version must be used. Let the distance between k and ω_m be δ , where $0 \leq \delta \leq \Delta k$. While it is possible to choose

the integration bounds in a manner such that the step which spans $|\omega_m|$ has $\delta = 0$, i.e., $|\omega_m|$ lies exactly on the boundary of the RG shell, it would be interesting to examine the dependence of the flow pattern on δ , over which the discrete flow equations are applied. For Methods 3 and 4, as $\delta \rightarrow 0$, the discrete equations can be readily shown to reduce to their corresponding differential equations. However, Method 2, has a “pathology” due to the horizontal sections of the RG shell and is therefore not possible to establish an equivalence with its continuous counterpart. In Fig. 7 we give a plot of the temperature dependence of the thermal mass parameter as a function of δ using Method 3. The corrections vanish in the limit $\delta \rightarrow 0$. Since having a large δ will destroy the exactness of the RG flow in the same way as having a large κ , one must always make δ as small as possible if not zero.

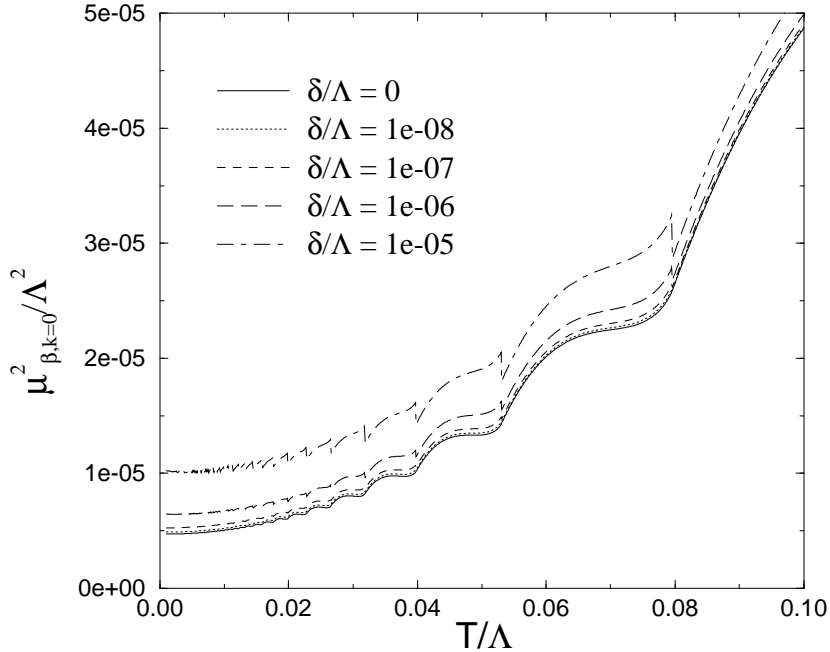


Figure 7. Dependence of $\mu_{\beta, k}^2$ on δ , using Method 3.

In Fig. 8 we plot the temperature dependence of the first six coupling constants at $k = 0$. All four schemes show excellent agreement up to oscillations. The oscillations obtained using Methods 2, 3, and 4 are due to the boundary conditions on the RG flow. For certain T , the constraint $\omega_{n_{max}} = \Lambda$ is satisfied exactly at $k = \Lambda$, while for others it is not. Technically speaking one should only compare data points which satisfy this constraint because different boundary conditions are mixed in the intermediate points and give rise to oscillations in the $g_{\beta, k}^{(2m)}$. The observed oscillations are a numerical artifact of the finiteness of the UV cutoff and signals the elimination of a particular $|\omega_n|$. A smooth curve may be obtained for methods 3 and 4 if we choose our UV cutoff Λ to be an integer multiple of T and set $\Delta k = 2\pi/\mathcal{N}\beta$ for some integer \mathcal{N} . Irrespective of this technicality, it is clear from Fig. 8 that all four methods give qualitatively the same results for the temperature dependence of coupling constants.

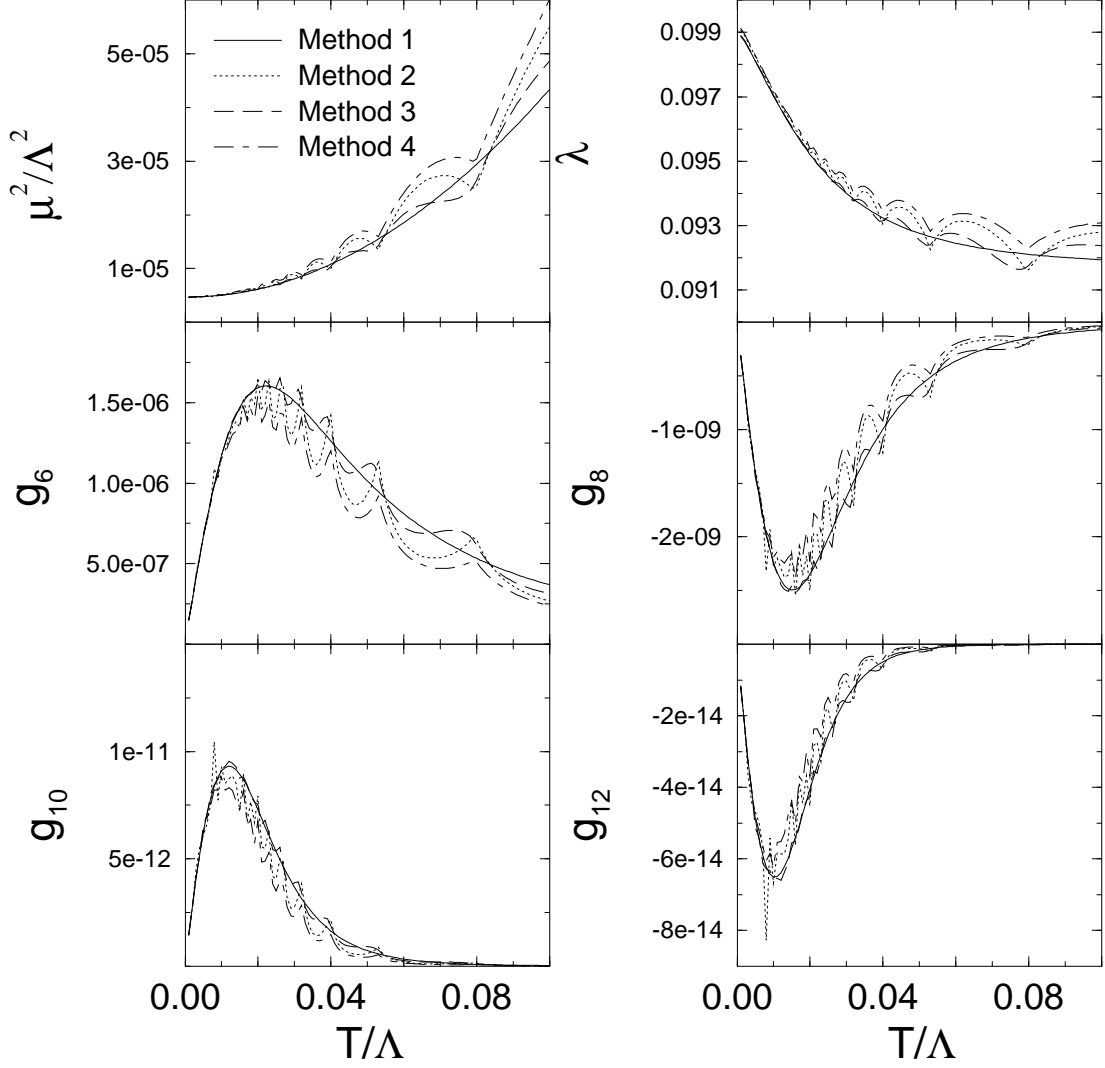


Figure 8. Temperature dependence of $g^{(2m)}$ in symmetric phase for $m=1,\dots,6$. The solid, dotted, dashed lines, and dot-dashed lines are for Methods 1, 2, 3, and 4 respectively.

Let us now examine more closely the MRG flow of the relevant coupling constants, namely, the mass parameter $\mu_{\beta,k}^2$ and the coupling constant $\lambda_{\beta,k}$. At finite temperature, according to the prediction of the one-loop perturbative approximation, the running mass parameter $\mu_\beta^2 = \mu_{\beta,k=0}^2$ exhibits a quadratic dependence on T . Applying the four RG schemes does not modify its strong T^2 dependence, i.e., incorporating the continuous feedback between the modes does not alter the temperature dependence of the thermal mass in the high- T limit.

The situation with the coupling constant $\lambda_\beta = \lambda_{\beta,k=0}$, unfortunately, has not been so clear. Its high-temperature behavior has been a subject of recent debate [4][8]. In this regime, a naive one-loop calculation breaks down completely and predicts that λ_β decreases and turns negative eventually. Including the two-loop contribution does not help either. Thus, RG remains the only tool which could shed light on the true behavior of λ_β . However, the results again differ depending on how RG is implemented and at what scale the coupling

constant is defined. In Ref. [8], for instance, it was claimed that when using Method 3, λ_β decreases at first, but then increases logarithmically. While the author attributed the discrepancy between his result and that of Ref. [4] based on Method 1 to the functional form of the smearing functions, we find that this is not the case. The actual cause of the discrepancy lies in the scale at which the coupling constants are defined, namely, in the former, $\lambda_{\beta,k=T}$ was considered, i.e., the coupling constant is defined at the scale $k = T$, whereas $\lambda_{\beta,k=0}$ was used in the latter. Had the normalization conditions agreed, the same result would have been obtained for all four RG schemes: $\lambda_{\beta,k=T}$ decreases, reaches a minimum, and then increases logarithmically. However, defining the coupling constant at $k = 0$ shows that $\lambda_{\beta,k=0}$ decreases and approximately approaches a constant for large T for all four methods.

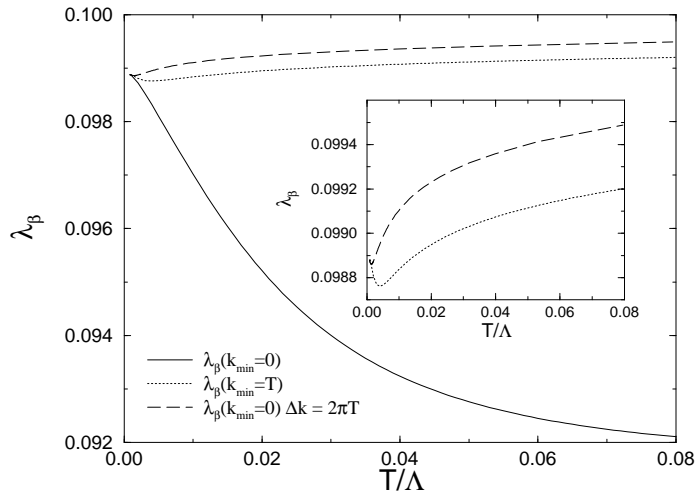


Figure 9. Comparison of $\lambda_{\beta,k}$ with different normalization conditions.

Certain methods, however, will yield erroneous temperature dependence of the coupling constants. An example is the Matsubara shell assumption in which a shell of thickness $\Delta k = 2\pi/\beta$ is integrated out in each step of the RG evolution. This assumption gives $\kappa \sim 1$ in the high T limit and the method breaks down completely (see Figure 9). In addition, this method yields mean field (four-dimensional) critical exponents instead of the Wilson-Fisher three-dimensional ones. For example, the exponent β , defined by $\Phi_{\beta,k} \sim |T - T_c(k)|^\beta$ as $\beta \rightarrow \beta_c(k)$, where $\Phi_{\beta,k}$ is the scale-dependent minimum of the potential [5], turns out to be $\beta = 1.01 \pm 0.01$ with the Matsubara-shell assumption.

We comment that the T dependence of the running parameters can also be examined from the point of view of the RG trajectories and the fixed-point structure of the theory. The presence of the infinite-temperature Gaussian fixed point implies that the RG trajectory must move in such a way that the fixed-point $(\mu_\beta^{2*}, \lambda_\beta^*) = (\infty, 0)$ is approached with increasing T . However, a careful analytical study reveals that the leading-order increment

of μ_β^2 is $\lambda_\beta T^2$, which means that the flow toward the fixed point must be slowed down as λ_β continues to decrease according to the coupled relations (see Appendix B):

$$\begin{aligned}\mu_\beta^2 &= \mu_R^2 + \frac{\lambda_\beta}{24\beta^2} - \frac{\lambda_\beta \bar{\mu}_\beta}{8\pi\beta^2} - \frac{\lambda_\beta \mu_\beta^2}{16\pi^2} \left[\ln\left(\frac{\bar{\mu}_\beta}{4\pi}\right) + \gamma - 1 \right] \\ \lambda_\beta &= \lambda_R - \frac{3\lambda_\beta^2}{16\pi\bar{\mu}_\beta} - \frac{3\lambda_\beta^2}{16\pi^2} \left[\ln\left(\frac{\bar{\mu}_\beta}{4\pi}\right) + \gamma \right],\end{aligned}\tag{3.2}$$

with $\bar{\mu}_\beta = \beta\mu_\beta$. The continuous feedback between μ_β^2 and λ_β in turn yields a slower convergence to their fixed point values. Since for a realistic system the attainment of $\mu_\beta^2 \rightarrow \infty$ is rather unlikely, the corresponding $\lambda_\beta \rightarrow 0$ limit will not be realized either. Therefore, it suffices to approximate λ_β by a constant.

Further argument against the increase of λ_β with T can also be made from the consideration of dimensional reduction, which takes place only if $\bar{\mu}_\beta \rightarrow 0$ in the limit of vanishing β [12]. As we have seen before, the quantity $\bar{\mu}_\beta$ is of order $\lambda_\beta^{1/2}$. Hence, if λ_β increases with T , $\bar{\mu}_\beta$ will also rise and the picture of high-temperature dimensional reduction will be destroyed completely.

$O(\Phi^{(2m)})$	γ	ν or ζ	$\lim_{k \rightarrow 0} \lambda_{\beta_c, k} T_c / \mu_{\beta_c, k}$
2	1.054 ± 0.005	0.527 ± 0.005	13.79 ± 0.05
3	1.171 ± 0.005	0.585 ± 0.005	29.35 ± 0.05
4	1.345 ± 0.005	0.672 ± 0.005	37.23 ± 0.05
5	1.504 ± 0.005	0.744 ± 0.005	38.78 ± 0.05
6	1.352 ± 0.005	0.675 ± 0.005	35.50 ± 0.05
7	1.312 ± 0.005	0.655 ± 0.005	35.20 ± 0.05

Table 1. Critical exponents and the effective coupling constant as a function of the level of polynomial truncation. Results for all four smearing functions are the same within the numerical accuracy. Errors reported here are due to numerics only and not that resulting from the polynomial truncation of the potential.

Other quantities can be measured to demonstrate the consistency of all four momentum blocking schemes. For example, one may examine the case $\mu_R^2 < 0$ where the symmetry is spontaneously broken. Although λ_β vanishes at criticality, the effective measure of the interaction is characterized, not by λ_β , but by $\lambda_3 \equiv \lim_{k \rightarrow 0} \lim_{T \rightarrow T_c} \lambda_{\beta, k} T / \mu_{\beta, k}$ which approaches a constant as $T \rightarrow T_c$. The effective coupling strength in the vicinity of transition is obtained using the polynomial expansion approximation up to Φ^{14} for MRG and the results are summarized in Table 1. We again find agreement in all four MRG equations within their numerical accuracy, and the results are comparable to those reported in Ref. [13]. In a similar manner, the critical exponents γ and ν were measured. From Table 1 we again see that all methods are consistent with one another. However, we caution the readers that these results will be less accurate than that obtained without polynomial truncation. This is because near criticality field amplitude fluctuations are strong, but such truncation applies only to the small fluctuation limit [5], [14].

IV. SUMMARY AND DISCUSSIONS

In this paper we have constructed finite-temperature RG equations for a scalar field theory in $S^1 \times R^d$ using a sharp momentum cutoff as the running parameter. We examined four different blocking schemes and illustrated how, with an infinitesimally small thickness of the RG shell, Δk , the feedback from the higher modes to the lower ones are systematically incorporated as they are integrated out. The smallness of the parameter $\kappa = \Delta k/k$, which represents the fraction of the modes that are eliminated in each blocking step, is the most crucial ingredient for the success of RG and constitutes the basis for the “exactness” of Eqs. (2.6), (2.14), (2.18) and (2.22), since corrections from higher loops are strongly suppressed by additional powers of κ .

The four MRG equations differ essentially in their treatment of the feedbacks between modes having the same $|\mathbf{p}|$ but different ω_n . In Method 1 the feedbacks are ignored entirely, but the trade-off is that its unconstrained summation over all n leads to a continuous RG. On the other hand, Methods 2, 3 and 4 which enforce certain couplings between $|\mathbf{p}|$ and ω_n do not lead to a differential function when there are non-vanishing contributions from eliminating the modes along the n -axis. However, for Methods 3 and 4, the differential forms are recovered by a judicious choice of Δk which puts all these points on the boundary of the RG shells. From the numerical results presented in Sec. III for the behavior of the n -point functions and the critical exponents, one finds remarkable agreement in all four methods, thus justifying the use of Method 1. We may therefore conclude that the couplings between different frequency modes with the same $|\mathbf{p}|$ may be safely ignored, provided that κ is chosen to be small. Had all the modes been strongly coupled, one would have to devise a laborious scheme which eliminates one degree of freedom at a time. Nevertheless, it remains an interesting question to see why an “independent-mode” approximation for n is sufficient for a small RG shell.

Knowing that physical properties are independent of the methodology of blocking, we find Method 1 to be most advantageous for numerical computation since it yields a continuous flow, with no oscillatory behavior in the high T limit. On the other hand, to examine the scaling behavior of the running parameters in the low T regime, Method 3 would be more convenient since it naturally leads back to the zero-temperature $(d+1)$ -dimensional theory.

Using the MRG (and TRG), we have examined the high-temperature behavior of coupling constant λ_β . Based on the fixed-point structure of the theory and the numerical results, it is clear that $\lambda_{\beta,k=0}$ must decrease with T but can be approximated by a positive constant in the limit $\bar{\mu}_\beta \ll 1$. The discrepancy in the literature concerning the behavior of $\lambda_{\beta,k}$ can be reconciled with a precise renormalization condition (viz, $k=0$ or $k=T$). We emphasize again that integrating out entire Matsubara shells at each RG step is ill-advised since it yields $\kappa \sim 1$ in the large T limit and the exactness of the RG flow is lost.

Various interesting directions can be pursued with our RG equations: Numerous critical exponents have been measured by Method 1 with the inclusion of wavefunction renormalization $Z_{\beta,k}(\Phi)$ in [5]. However, the accuracy in the polynomial expansion can certainly be improved. Derivations of the RG equation for $Z_{\beta,k}(\Phi)$ using Methods 2, 3 and 4 can also provide a consistency check with Method 1 [15]. It would also be interesting to compare our predictions for the universal amplitude ratios with those obtained using the ϵ

expansion and the lattice methods. The one-component RG equation Eq. (2.6) can readily be generalized to N components:

$$k \frac{dU_{\beta,k}(\Phi)}{dk} = -\frac{S_d k^d}{2\beta} \left\{ (N-1) \left(\beta \sqrt{k^2 + U'_{\beta,k}(\Phi)} + 2 \ln \left[1 - e^{-\beta \sqrt{k^2 + U'_{\beta,k}(\Phi)}} \right] \right) \right. \\ \left. + \beta \sqrt{k^2 + U'_{\beta,k}(\Phi) + U''_{\beta,k}(\Phi) \Phi^2} + 2 \ln \left[1 - e^{-\beta \sqrt{k^2 + U'_{\beta,k}(\Phi) + U''_{\beta,k}(\Phi) \Phi^2}} \right] \right\}, \quad (4.1)$$

where the prime notation now denotes the differentiation with respect to $\Phi^2/2 = \Phi^a \Phi^a/2$ with $a = 1, \dots, N$. Critical exponents corresponding to the XY ($N = 2$) model and Heisenberg ($N = 3$) model can now be extracted in a similar manner. In addition, the equation may also provide information on the interplay between the longitudinal and the transverse Goldstone modes. One may also explore different IR scaling regimes and search for the possible non-universal behavior which may arise due to the emergence of new relevant operators that are suppressed in the UV scaling regions [16]. Nonperturbative modification of the scaling laws due to the presence of a condensate can also be addressed. Gauge theories, too, can also be further investigated [17] [18]. These issues will be presented in forthcoming publications.

ACKNOWLEDGMENTS

S.-B. L. is grateful to J. Polonyi, V. Branchina, J. Alexandre and A. Bodor for stimulating discussions. M.S. would like to thank D. Furnstahl and E. Braaten for discussions as well. This work is supported in part by funds provided by the National Science Council of Taiwan under contract #NSC-87-2112-M-194-004, and by the National Science Foundation under Grants No. PHY-9511923 and PHY-9258270.

APPENDIX A. TEMPERATURE RENORMALIZATION GROUP

In Sec II, the MRG prescription was explored from the point of view of momentum space construction using an IR cutoff k as the running parameter. The external variable, temperature, has been taken as an input parameter. To examine the behavior of a physical system at finite temperature, there exists an alternative temperature renormalization group (TRG), in which β , the inverse of temperature, plays the role of the flow parameter [19]. TRG provides a direct investigation of the response of a system when T is varied. Quantities at different T and fixed k can also be related to each other by this finite renormalization procedure.

To construct the TRG flow equation, we again begin with the perturbative one-loop expression for the blocked potential given in Eq. (2.3). Differentiating the expression with respect to β yields

$$\beta \frac{\partial \tilde{U}_{\beta,k}}{\partial \beta} = - \int'_{\mathbf{p}} \left\{ \frac{1}{\beta} \ln \sinh \left(\frac{\beta \sqrt{\mathbf{p}^2 + V''}}{2} \right) - \frac{\sqrt{\mathbf{p}^2 + V''}}{2} \coth \left(\frac{\beta \sqrt{\mathbf{p}^2 + V''}}{2} \right) \right\}. \quad (\text{A.1})$$

By varying β infinitesimally from $\beta \rightarrow \beta - \Delta\beta$, i.e., the system is heated up gradually until the desired temperature scale is reached, we arrive at the following improved TRG equation:

$$\begin{aligned} \beta \frac{\partial U_{\beta,k}}{\partial \beta} = & - \int'_{\mathbf{p}} \left\{ \frac{1}{\beta} \ln \sinh \left(\frac{\beta \sqrt{\mathbf{p}^2 + U''_{\beta,\mathbf{p}}}}{2} \right) \right. \\ & \left. - \frac{1}{2} \left[\sqrt{\mathbf{p}^2 + U''_{\beta,\mathbf{p}}} + \beta \frac{\partial}{\partial \beta} \sqrt{\mathbf{p}^2 + U''_{\beta,\mathbf{p}}} \right] \coth \left(\frac{\beta \sqrt{\mathbf{p}^2 + U''_{\beta,\mathbf{p}}}}{2} \right) \right\}. \end{aligned} \quad (\text{A.2})$$

By assuming a small RG shell for the $|\mathbf{p}|$ integration, or equivalently, $k = \Lambda - \Delta k$, higher loop corrections again are suppressed.

One can readily verify the equivalence between the TRG and the MRG formalisms by observing that the same expression

$$\begin{aligned} k \frac{\partial}{\partial k} \left(\beta \frac{\partial U_{\beta,k}}{\partial \beta} \right) = & S_d k^d \left\{ \frac{1}{\beta} \ln \sinh \left(\frac{\beta \sqrt{k^2 + U''_{\beta,k}}}{2} \right) \right. \\ & \left. - \frac{1}{2} \left[\sqrt{k^2 + U''_{\beta,k}} + \beta \frac{\partial}{\partial \beta} \sqrt{k^2 + U''_{\beta,k}} \right] \coth \left(\frac{\beta \sqrt{k^2 + U''_{\beta,k}}}{2} \right) \right\}, \end{aligned} \quad (\text{A.3})$$

is obtained by differentiating (A.2) with respect to $\ln k$ or (2.6) with respect to $\ln \beta$. However, since Eq. (A.2) is an integro-differential equation, direct numerical solution is more cumbersome than the MRG equations. Notice that for large β , the results derived from (A.2) and (A.1) should not differ appreciably. However, in the small β regime, Eq. (A.1), which is derived using the independent-mode approximation, fails completely.

The β dependence of the running parameters in the coupling constant space can be examined by differentiating (A.2) with respect to Φ and setting $\Phi = 0$. To $O(\lambda_{\beta,k})$, we have

$$\begin{aligned} \beta \frac{\partial \mu_{\beta,k}^2}{\partial \beta} = & -\frac{\beta}{8} \int'_{\mathbf{p}} \text{csch}^2 \left(\frac{\sqrt{\mathbf{p}^2 + \mu_{\beta,\mathbf{p}}^2}}{2} \right) \left\{ \lambda_{\beta,\mathbf{p}} - \frac{1}{\sqrt{\mathbf{p}^2 + \mu_{\beta,\mathbf{p}}^2}} \left(\frac{\partial \lambda_{\beta,\mathbf{p}}}{\partial \beta} \right) \sinh \left(\sqrt{\mathbf{p}^2 + \mu_{\beta,\mathbf{p}}^2} \right) \right. \\ & \left. + \frac{\beta \lambda_{\beta,\mathbf{p}}}{2(\mathbf{p}^2 + \mu_{\beta,\mathbf{p}}^2)} \left(\frac{\partial \mu_{\beta,\mathbf{p}}^2}{\partial \beta} \right) \left[1 + \frac{1}{\beta \sqrt{\mathbf{p}^2 + \mu_{\beta,\mathbf{p}}^2}} \sinh \left(\beta \sqrt{\mathbf{p}^2 + \mu_{\beta,\mathbf{p}}^2} \right) \right] \right\} + \text{C.T.}, \end{aligned} \quad (\text{A.4})$$

$$\begin{aligned}
\beta \frac{\partial \lambda_{\beta,k}}{\partial \beta} = & -\frac{3\beta^2}{16} \int_{\mathbf{p}}' \frac{\lambda_{\beta,\mathbf{p}}}{\sqrt{\mathbf{p}^2 + \mu_{\beta,\mathbf{p}}^2}} \operatorname{csch}^2\left(\frac{\beta\sqrt{\mathbf{p}^2 + \mu_{\beta,\mathbf{p}}^2}}{2}\right) \left\{ \frac{\lambda_{\beta,\mathbf{p}}}{\beta\sqrt{\mathbf{p}^2 + \mu_{\beta,\mathbf{p}}^2}} \right. \\
& - \lambda_{\beta,\mathbf{p}} \coth\left(\frac{\beta\sqrt{\mathbf{p}^2 + \mu_{\beta,\mathbf{p}}^2}}{2}\right) + \frac{2}{\sqrt{\mathbf{p}^2 + \mu_{\beta,\mathbf{p}}^2}} \left(\frac{\partial \lambda_{\beta,\mathbf{p}}}{\partial \beta}\right) \\
& \left. - \frac{\beta \lambda_{\beta,\mathbf{p}}}{(\mathbf{p}^2 + \mu_{\beta,\mathbf{p}}^2)} \left(\frac{\partial \mu_{\beta,\mathbf{p}}^2}{\partial \beta}\right) \left[\frac{1}{\beta\sqrt{\mathbf{p}^2 + \mu_{\beta,\mathbf{p}}^2}} + \frac{1}{2} \coth\left(\frac{\beta\sqrt{\mathbf{p}^2 + \mu_{\beta,\mathbf{p}}^2}}{2}\right) \right] \right\} + \text{C.T.},
\end{aligned} \tag{A.5}$$

where C.T. denotes the appropriate counterterms needed to subtract off the divergences in the momentum integration. Note that these counterterms are necessarily temperature-dependent [20].

Unfortunately, the coupled integro-differential equations are still too difficult to be solved exactly; even analytical approximations are restricted only to certain regimes. However, in the high-temperature regime where β is small, we ignore the \mathbf{p} dependence in the mass and coupling constants and obtain

$$\begin{aligned}
& \beta \frac{\partial \mu_{\beta}^2}{\partial \beta} \left\{ 1 + \frac{\lambda_{\beta}\beta}{16} \int_{\mathbf{p}} \frac{1}{\mathbf{p}^2 + \mu_{\beta}^2} \left[1 + \frac{1}{\beta\sqrt{\mathbf{p}^2 + \mu_{\beta}^2}} \sinh\left(\beta\sqrt{\mathbf{p}^2 + \mu_{\beta}^2}\right) \right] \operatorname{csch}^2\left(\frac{\beta\sqrt{\mathbf{p}^2 + \mu_{\beta}^2}}{2}\right) \right\} \\
& = -\frac{\lambda_{\beta}\beta}{8} \int_{\mathbf{p}} \operatorname{csch}^2\left(\frac{\beta\sqrt{\mathbf{p}^2 + \mu_{\beta}^2}}{2}\right) \left\{ \lambda_{\beta} - \frac{1}{\sqrt{\mathbf{p}^2 + \mu_{\beta}^2}} \left(\frac{\partial \lambda_{\beta}}{\partial \beta}\right) \sinh\left(\beta\sqrt{\mathbf{p}^2 + \mu_{\beta}^2}\right) \right\} + \text{C.T.},
\end{aligned} \tag{A.6}$$

and

$$\begin{aligned}
& \beta \frac{\partial \lambda_{\beta}}{\partial \beta} \left\{ 1 + \frac{3\lambda_{\beta}\beta}{8} \int_{\mathbf{p}} \frac{1}{\mathbf{p}^2 + \mu_{\beta}^2} \operatorname{csch}^2\left(\frac{\beta\sqrt{\mathbf{p}^2 + \mu_{\beta}^2}}{2}\right) \right\} \\
& = -\frac{3\lambda_{\beta}^2\beta^2}{16} \int_{\mathbf{p}} \frac{1}{\sqrt{\mathbf{p}^2 + \mu_{\beta}^2}} \operatorname{csch}^2\left(\frac{\beta\sqrt{\mathbf{p}^2 + \mu_{\beta}^2}}{2}\right) \left\{ \frac{1}{\beta\sqrt{\mathbf{p}^2 + \mu_{\beta}^2}} - \coth\left(\beta\sqrt{\mathbf{p}^2 + \mu_{\beta}^2}\right) \right. \\
& \quad \left. - \frac{1}{\mathbf{p}^2 + \mu_{\beta}^2} \left[\frac{1}{\beta\sqrt{\mathbf{p}^2 + \mu_{\beta}^2}} + \frac{1}{2} \coth\left(\beta\sqrt{\mathbf{p}^2 + \mu_{\beta}^2}\right) \right] \right\} + \text{C.T.},
\end{aligned} \tag{A.7}$$

for vanishing k . The above two RG equations will allow us to examine the fixed-point structure of the theory, as we shall see in Appendix B.

APPENDIX B. RENORMALIZATION GROUP AND THE FIXED POINTS

The complicated RG flow can be greatly simplified in the neighborhood of fixed points where a linearized RG prescription becomes possible and only the relevant operators need to be retained. The irrelevant operators can be safely ignored. The classification of relevancy, however, depends on the fixed point; what is relevant around a particular fixed point may turn irrelevant as it flows into another one. Thus, the linearized prescription may be used only when the system is sufficiently close to a fixed point. To describe the flow further away from the fixed point, a global nonlinear RG analysis is generally required. Once all the fixed points are located, the general RG flow of the theory can be mapped out. Below we examine the fixed-point structure of both MRG and TRG.

1. MRG Approach

For MRG, we shall work with Method 1 since its RG evolution is continuous. It is convenient to employ the dimensionless quantities:

$$\begin{aligned}\bar{U}_{\beta,k}(\bar{\Phi}) &= \beta k^{-d} U_{\beta,k}(\Phi), & \bar{\Phi} &= \beta^{1/2} k^{-(d-2)/2} \Phi, \\ \bar{U}_{\beta,k}^{(m)}(\bar{\Phi}) &= \frac{\partial^m \bar{U}_{\beta,k}(\bar{\Phi})}{\partial \bar{\Phi}^m} = \beta^{1-m/2} k^{-d+m(d-2)/2} U_{\beta,k}^{(m)}(\Phi), \\ \bar{\mu}_{\beta,k}^2 &= \bar{U}_{\beta,k}^{(2)}(0) = k^{-2} \mu_{\beta,k}^2, & \bar{\lambda}_{\beta,k} &= \bar{U}_{\beta,k}^{(4)}(0) = \beta^{-1} k^{d-4} \lambda_{\beta,k},\end{aligned}\tag{B.1}$$

where, for the purpose of the present paper, we set the anomalous dimension η to be zero. Eq. (2.6) can now be written as

$$\left[k \partial_k - \frac{1}{2} (d-2) \bar{\Phi} \partial_{\bar{\Phi}} + d \right] \bar{U}_{\beta,k} = -\frac{S_d}{2} \left\{ \bar{\beta} \sqrt{1 + \bar{U}_{\beta,k}''} + 2 \ln [1 - e^{-\bar{\beta} \sqrt{1 + \bar{U}_{\beta,k}''}}] \right\}, \tag{B.2}$$

which implies the following fixed-point equation:

$$-\frac{1}{2} (d-2) \bar{\Phi} \bar{U}_{\beta,k}^{*'} + d \bar{U}_{\beta,k}^* = -\frac{S_d}{2} \left\{ \bar{\beta} \sqrt{1 + \bar{U}_{\beta,k}^{*''}} + 2 \ln [1 - e^{-\bar{\beta} \sqrt{1 + \bar{U}_{\beta,k}^{*''}}}] \right\}, \tag{B.3}$$

with $\bar{U}_{\beta,k}^*(\bar{\Phi})$ being the fixed-point potential. However, by making a polynomial expansion of the blocked potential $U_{\beta,k}(\bar{\Phi})$ and keeping track of only the evolution of the leading-order $\bar{\mu}_{\beta,k}^2$ and $\bar{\lambda}_{\beta,k}$, it is possible to identify the fixed points on the $(\bar{\mu}_{\beta,k}^2, \bar{\lambda}_{\beta,k})$ plane. Consistency with reflection symmetry around the origin demands that only even-power terms are present and we have

$$\bar{U}_{\beta,k}(\bar{\Phi}) = \sum_{m=1}^{\infty} \frac{\bar{g}_{\beta,k}^{(2m)}}{(2m)!} \bar{\Phi}^{2m}, \quad \bar{g}_{\beta,k}^{(2m)} = \bar{U}_{\beta,k}^{(2m)}(0), \tag{B.4}$$

with $\bar{g}_{\beta,k}^{(2)} = \bar{\mu}_{\beta,k}^2$ and $\bar{g}_{\beta,k}^{(4)} = \bar{\lambda}_{\beta,k}$.

In the high-temperature limit where $\bar{\beta} \ll 1$, the manifold changes from $S^1 \times R^d$ to R^d , exhibiting a critical behavior governed by the d -dimensional fixed point. Thus, one expects

$$\bar{\beta} \rightarrow 0 : \quad \begin{cases} S^1 \times R^d \longrightarrow R^d \\ \bar{\Phi} \longrightarrow \bar{\Phi}_d & (\Phi \longrightarrow \beta^{-1/2} \Phi_d) \\ \bar{U}_{\beta,k} \longrightarrow \bar{U}_{k,d} & (U_{\beta,k} \longrightarrow \beta^{-1} U_{k,d}) \\ \bar{g}_{\beta,k}^{(m)} \longrightarrow \bar{g}_{k,d}^{(m)} & (g_{\beta,k}^{(m)} \longrightarrow \beta^{m/2-1} g_{k,d}^{(m)}) , \end{cases} \quad (\text{B.5})$$

and

$$\left[k \partial_k - \frac{1}{2} (d-2) \bar{\Phi}_d \partial_{\bar{\Phi}_d} + d \right] \bar{U}_{k,d}(\bar{\Phi}_d) = -\frac{S_d}{2} \ln \left[\frac{1 + \partial_{\bar{\Phi}_d}^2 \bar{U}_{k,d}(\bar{\Phi}_d)}{1 + \partial_{\bar{\Phi}_d}^2 \bar{U}_{k,d}(0)} \right]. \quad (\text{B.6})$$

Concentrating only on the running of $\bar{\mu}_{\beta,k}^2$ and $\bar{\lambda}_{\beta,k}$, the evolution equations can be approximated as

$$\begin{aligned} k \frac{\partial \bar{\mu}_{k,d}^2}{\partial k} &= -2 \bar{\mu}_{k,d}^2 - \frac{\bar{\lambda}_{k,d} S_d}{2(1 + \bar{\mu}_{k,d}^2)} \\ k \frac{\partial \bar{\lambda}_{k,d}}{\partial k} &= -(4-d) \bar{\lambda}_{k,d} + \frac{3 \bar{\lambda}_{k,d}^2 S_d}{2(1 + \bar{\mu}_{k,d}^2)^2}. \end{aligned} \quad (\text{B.7})$$

If we further define

$$\bar{r} = \frac{\bar{\mu}_{k,d}^2}{1 + \bar{\mu}_{k,d}^2}, \quad \bar{\ell} = \frac{\bar{\lambda}_{k,d}}{(1 + \bar{\mu}_{k,d}^2)^2}, \quad (\text{B.8})$$

Eq. (B.7) then simplifies to

$$\begin{aligned} k \frac{\partial \bar{r}}{\partial k} &= -(1 - \bar{r})(2\bar{r} + \frac{S_d}{2} \bar{\ell}) \\ k \frac{\partial \bar{\ell}}{\partial k} &= -\bar{\ell} \left(\epsilon - 4\bar{r} - \frac{5S_d}{2} \bar{\ell} \right), \end{aligned} \quad (\text{B.9})$$

where $\epsilon = 4 - d$. Fixed points can now be located. There are two trivial fixed points of Gaussian nature located at $(\bar{r}^*, \bar{\ell}^*) = (0, 0)$ and $(1, 0)$. The former is the usual trivial “finite” Gaussian fixed point at which all running parameters vanish. On the other hand, the latter describes an infinite (temperature) Gaussian fixed point which can only be reached when $T \rightarrow \infty$. In addition, for $D = d < 4$ or $\epsilon > 0$, we have the IR Wilson-Fisher (WF) fixed point $(\bar{r}^*, \bar{\ell}^*) = (-\epsilon/6, 2\epsilon/3S_d)$ [21], which coincides with the usual trivial Gaussian fixed point for $\epsilon = 0$. Thus, we have $\bar{\ell}^* = 16\pi^2\epsilon/3$ for $d = 4$. While Eq. (B.9) is already diagonal around the infinite Gaussian fixed point, it is possible to introduce the new variables [22]

$$\bar{x} = \frac{3S_d}{2} \bar{\ell}, \quad \bar{y} = \bar{r} + \frac{S_d}{2(2 - \epsilon)} \bar{\ell}, \quad (\text{B.10})$$

and transform (B.9) into

$$\begin{aligned} k \frac{\partial \bar{x}}{\partial k} &= -\bar{x} \left[\epsilon(1 - \bar{x}) - 4\bar{y} \right] \\ k \frac{\partial \bar{y}}{\partial k} &= 2\bar{y} \left(\bar{y} - 1 - \frac{\epsilon \bar{x}}{6} \right) + O(\epsilon^2 \bar{x}^2). \end{aligned} \quad (\text{B.11})$$

The new expression is now diagonalized around the finite Gaussian fixed point $(0, 0)$, with the infinite Gaussian and the WF fixed points located, respectively, at $(0, 1)$ and $(1, 0)$ on the (\bar{x}, \bar{y}) plane.

On the other hand, in the low T limit, one expects

$$\bar{\beta} \rightarrow \infty : \begin{cases} S^1 \times R^d \longrightarrow R^{d+1} \\ \bar{\Phi} \longrightarrow \bar{\beta}^{1/2} \bar{\Phi}_{d+1} & (\Phi \longrightarrow \Phi_{d+1}) \\ \bar{U}_{\beta,k} \longrightarrow \bar{\beta}^{-1} \bar{U}_{k,d+1} & (U_{\beta,k} \longrightarrow U_{k,d+1}) \\ \bar{g}_{\beta,k}^{(m)} \longrightarrow \bar{\beta}^{1-m/2} \bar{g}_{k,d+1}^{(m)} & (g_{\beta,k}^{(m)} \longrightarrow g_{k,d+1}^{(m)}) \end{cases} \quad (\text{B.12})$$

and

$$\left[k \partial_k - \frac{1}{2} (d-2) \bar{\Phi} \partial_{\bar{\Phi}} + d \right] \bar{U}_{k,d+1}(\bar{\Phi}) = -\frac{S_d \bar{\beta}}{2} \sqrt{1 + \partial_{\bar{\Phi}}^2 \bar{U}_{k,d+1}(\bar{\Phi})}, \quad (\text{B.13})$$

which yields

$$\begin{aligned} k \frac{\partial \bar{\mu}_{k,d+1}^2}{\partial k} &= -2 \bar{\mu}_{k,d+1}^2 - \frac{\bar{\lambda}_{k,d+1} S_d}{4(1 + \bar{\mu}_{k,d+1}^2)^{1/2}} \\ k \frac{\partial \bar{\lambda}_{k,d+1}}{\partial k} &= -(3-d) \bar{\lambda}_{k,d+1} + \frac{3 \bar{\lambda}_{k,d+1}^2 S_d}{8(1 + \bar{\mu}_{k,d+1}^2)^{3/2}}. \end{aligned} \quad (\text{B.14})$$

Here we see that the only fixed point is the trivial finite Gaussian $(\bar{\mu}_{k,d+1}^{2*}, \bar{\lambda}_{k,d+1}^*) = (0, 0)$, for $d \geq 3$. While the finite Gaussian fixed point can be accessed in both low and high T regimes, the WF and the infinite Gaussian fixed points are reachable only in the large T limit. The rationale for the inability to detect these two fixed points at low T is that they are characteristic of R^d with $d < 4$, and yet the effective manifold is R^{d+1} for small T .

2. TRG Approach

The fixed-point structure associated with the flow of TRG can be examined in a similar manner. We focus again only on the evolution of the leading-order running coupling constants μ_β^2 and λ_β at $k = 0$. To simplify the task of solving the coupled integro-differential equations Eqs. (A.6) and (A.7), we choose the manifold to be $S^1 \times R^3$ for definiteness.

In the limit $\bar{\beta} \mu_\beta \ll 1$, the RG equations can be approximated as

$$\begin{aligned} \beta \frac{\partial \mu_\beta^2}{\partial \beta} &= \frac{\mu_\beta^2}{4\pi^2} \left\{ \lambda_\beta \bar{\mu}_\beta \frac{\partial F_1(\bar{\mu}_\beta)}{\partial \bar{\mu}_\beta} + \beta \frac{\partial \lambda_\beta}{\partial \beta} F_1(\bar{\mu}_\beta) \right\} \\ &= -\frac{1}{12\beta^2} \left\{ \lambda_\beta \left(1 - \frac{\bar{\mu}_\beta}{2\pi} + \frac{3\bar{\mu}_\beta^2}{4\pi^2} \right) - \beta \frac{\partial \lambda_\beta}{\partial \beta} \left(\frac{1}{2} - \frac{3\bar{\mu}_\beta}{2\pi} \right) + \dots \right\}, \end{aligned} \quad (\text{B.15})$$

and

$$\beta \frac{\partial \lambda_\beta}{\partial \beta} = -\frac{3\lambda_\beta^2 \beta}{16\pi^2 \mu_\beta} \left(\beta \frac{\partial \mu_\beta^2}{\partial \beta} + 2\mu_\beta^2 \right) \frac{\partial F_2(\bar{\mu}_\beta)}{\partial \bar{\mu}_\beta} = -\frac{3\lambda_\beta^2}{32\pi^2 \mu_\beta^2} \left(\beta \frac{\partial \mu_\beta^2}{\partial \beta} + 2\mu_\beta^2 \right) \left(1 - \frac{\pi}{\bar{\mu}_\beta} \right) + \dots \quad (\text{B.16})$$

where

$$\begin{aligned} \int_{\mathbf{p}} \text{csch}^2\left(\frac{\beta\sqrt{\mathbf{p}^2 + \mu_\beta^2}}{2}\right) &= -\frac{2\mu_\beta^3}{\pi^2} \frac{\partial F_1(\bar{\mu}_\beta)}{\partial \bar{\mu}_\beta}, \\ \int_{\mathbf{p}} \frac{1}{\sqrt{\mathbf{p}^2 + \mu_\beta^2}} \coth\left(\frac{\beta\sqrt{\mathbf{p}^2 + \mu_\beta^2}}{2}\right) &= \frac{\mu_\beta^2}{\pi^2} F_1(\bar{\mu}_\beta) + \dots, \end{aligned} \quad (\text{B.17})$$

and [23]

$$\begin{aligned} F_1(\bar{\mu}_\beta) &= \int_0^\infty \frac{dy}{\sqrt{y^2 + 1}} \frac{y^2}{e^{\bar{\mu}_\beta \sqrt{y^2 + 1}} - 1} = \frac{2\pi^2}{\bar{\mu}_\beta^2} \left[\frac{1}{12} - \frac{\bar{\mu}_\beta}{4\pi} - \frac{\bar{\mu}_\beta^2}{8\pi^2} \ln \bar{\mu}_\beta + \dots \right], \\ \frac{\partial F_1(\bar{\mu}_\beta)}{\partial \bar{\mu}_\beta} &= - \int_0^\infty dy \frac{y^2 e^{\bar{\mu}_\beta \sqrt{y^2 + 1}}}{(e^{\bar{\mu}_\beta \sqrt{y^2 + 1}} - 1)^2} = -\frac{\pi^2}{3\bar{\mu}_\beta^3} \left[1 - \frac{\bar{\mu}_\beta}{2\pi} + \frac{3\bar{\mu}_\beta^2}{4\pi^2} + \dots \right], \\ F_2(\bar{\mu}_\beta) &= \int_0^\infty \frac{dy}{\sqrt{y^2 + 1}} \frac{1}{e^{\bar{\mu}_\beta \sqrt{y^2 + 1}} - 1} = \frac{1}{2} \ln \bar{\mu}_\beta + \frac{\pi}{2\bar{\mu}_\beta} + \dots, \\ \frac{\partial F_2(\bar{\mu}_\beta)}{\partial \bar{\mu}_\beta} &= - \int_0^\infty dy \frac{e^{\bar{\mu}_\beta \sqrt{y^2 + 1}}}{(e^{\bar{\mu}_\beta \sqrt{y^2 + 1}} - 1)^2} = \frac{1}{2\bar{\mu}_\beta} \left(1 - \frac{\pi}{\bar{\mu}_\beta} \right) + \dots. \end{aligned} \quad (\text{B.18})$$

Note that β is now the running parameter of the RG. One may actually derive the above evolution equations by differentiating the coupled self-consistent equations

$$\begin{aligned} \mu_\beta^2 &= \mu_R^2 + \frac{\lambda_\beta}{24\beta^2} - \frac{\lambda_\beta \bar{\mu}_\beta}{8\pi\beta^2} - \frac{\lambda_\beta \mu_\beta^2}{16\pi^2} \left[\ln\left(\frac{\bar{\mu}_\beta}{4\pi}\right) + \gamma - 1 \right] \\ \lambda_\beta &= \lambda_R - \frac{3\lambda_\beta^2}{16\pi\bar{\mu}_\beta} - \frac{3\lambda_\beta^2}{16\pi^2} \left[\ln\left(\frac{\bar{\mu}_\beta}{4\pi}\right) + \gamma \right], \end{aligned} \quad (\text{B.19})$$

which are valid for a small but positive $\bar{\mu}_\beta$ [5].

Upon substituting the familiar leading-order result

$$\beta \frac{\partial \mu_\beta^2}{\partial \beta} = -\frac{\lambda_\beta}{12\beta^2} + \dots, \quad \text{or} \quad \mu_\beta^2 = \mu_R^2 + \frac{\lambda_\beta}{24\beta^2} + \dots, \quad (\text{B.20})$$

into Eq. (B.16), the fixed points may now be located by solving

$$0 = \beta \frac{\partial \lambda_\beta}{\partial \beta} = -\frac{3\lambda_\beta^2}{16\pi^2} \left(1 - \frac{\lambda_\beta}{24\bar{\mu}_\beta^2} \right) \left(1 - \frac{\pi}{\bar{\mu}_\beta} \right). \quad (\text{B.21})$$

Since the equation is derived for $\bar{\mu}_\beta \ll 1$, we require $\bar{\mu}_\beta < \pi$. Two fixed points may now be located. The first one is the usual trivial finite Gaussian fixed point $(\mu_\beta, \lambda_\beta) = (0, 0)$. As for the second one, we see that for $\lambda_\beta/24\bar{\mu}_\beta^2 \rightarrow 1$, or equivalently $\beta \rightarrow 0$, the theory approaches the infinite Gaussian fixed point $(\mu_\beta, \lambda_\beta) = (\infty, 0)$. Its Gaussian nature is

readily seen by noting that $\bar{\mu}_\beta \sim \lambda_\beta^{1/2}$, and thus, when $\mu_\beta \rightarrow \infty$ and $\beta \rightarrow 0$ such that $\bar{\mu}_\beta \rightarrow 0$, λ_β must be vanishingly small.

In general one may regard phase transitions as a “high-temperature” phenomenon since $\mu_\beta \rightarrow 0$ in the vicinity of criticality. Although we are able to detect two Gaussian fixed points, the important WF fixed point which characterizes the critical behavior of the system seems to be missing. A crucial observation here is that in the large T regime one expects the effective degrees of freedom to crossover from four-dimensional to three-dimensional, and hence λ_β is not an accurate measure of the effective interaction strength of the theory. Instead, the interaction is accounted for by $\lambda_{\beta,3} = \lambda_\beta T$, or $\bar{\lambda}_{\beta,3} = \lambda_\beta / \bar{\mu}_\beta$ in the dimensionless form. Thus, in terms of $\bar{\mu}_\beta$ and $\bar{\lambda}_{\beta,3}$, we have

$$\begin{aligned} \beta \frac{\partial \bar{\mu}_\beta}{\partial \beta} &= \bar{\mu}_\beta - \frac{\bar{\lambda}_{\beta,3}}{24} \\ \beta \frac{\partial \bar{\lambda}_{\beta,3}}{\partial \beta} &= -\bar{\lambda}_{\beta,3} \left(1 - \frac{\bar{\lambda}_{\beta,3}}{24\bar{\mu}_\beta} \right) \left[1 + \frac{3\bar{\lambda}_{\beta,3}\bar{\mu}_\beta}{16\pi^2} \left(1 - \frac{\pi}{\bar{\mu}_\beta} \right) \right]. \end{aligned} \quad (\text{B.22})$$

The much richer structure associated with the flow of $\bar{\lambda}_{\beta,3}$ now reveals the existence of the additional nontrivial fixed point. Besides the usual finite $(0,0)$ and infinite Gaussian $(1,0)$, we have, keeping only the leading-order contribution in the bracket,

$$(\bar{\mu}_\beta^*, \bar{\lambda}_{\beta,3}^*) = \left(\frac{2\pi}{9}, \frac{16\pi}{3} \right), \quad (\text{B.23})$$

The numerical value for $\bar{\lambda}_{\beta,3}^*$ can be compared with that tabulated in [13]. Therefore, contrary to the well known notion of triviality for $T = 0$ at dimensionality $D = 4$, the theory in the high T limit is seen to crossover to an interacting theory characterized by a nontrivial fixed point of $D = 3$.

We comment that in the TRG formalism, by first taking the limit $k \rightarrow 0$ in Eqs. (A.4) and (A.5), we are left with one arbitrary parameter β , the circumference of the submanifold S^1 , with all other dimensions being infinite. Since any TRG transformation now formally corresponds to changing the value of β , it is natural to expect the extrema $\beta = 0$ and $\beta = \infty$ to be fixed points that characterize, respectively, the three-dimensional and four-dimensional limits of the theory. While $D = 4$ for $\bar{\mu}_\beta \gg 1$, it becomes three in the limit $\bar{\mu}_\beta \ll 1$. Therefore, the dimensional crossover scale in this TRG formalism can be given qualitatively as $\bar{\mu}_\beta \sim 1$. This implies that when $\bar{\mu}_\beta$ falls below unity new effective three-dimensional degrees of freedom need to be employed in order to give a correct account of the theory. However, had the new degrees of freedom associated with $D = 3$ not been used, the WF fixed point would be missed. In fact, the success of a given RG scheme in characterizing the crossover phenomenon is attributed to its capability of tracking the effective degrees of freedom. We also note that the method of resumming daisy and superdaisy diagrams proposed by Dolan and Jackiw [24] is similar to TRG; however, the important distinction is that in the former approach, the coupling constant has always been fixed at its zero-temperature renormalized value and consequently, the prescription only gives the two Gaussian fixed points and yields the mean-field exponents. Thus, we see that only when the running of the effective coupling constant $\bar{\lambda}_{\beta,k}$ is taken into account can one access the nontrivial WF fixed point.

REFERENCES

- [1] S.-B. Liao, J. Polonyi and D. P. Xu, *Phys. Rev.* **D51** (1995) 748.
- [2] see, for example, D. Dalvit and F. Mazzitelli, *Phys. Rev.* **D54** (1996) 6338;
M. D’Attanasio and M. Pietroni, *Nucl. Phys.* **B472** (1996) 711;
K. Ogure and J. Sato, hep-ph/9801439 and hep-ph/9802418;
N. Tetradis and C. Wetterich, *Nucl. Phys.* **B422** (1994) 541.
- [3] K. Wilson, *Phys. Rev.* **B4** (1971) 3174; K. Wilson and J. Kogut, *Phys. Rep.* **12C** (1975) 75.
- [4] S.-B. Liao and M. Strickland, *Phys. Rev.* **D52** (1995) 3653.
- [5] S.-B. Liao and M. Strickland, *Nucl. Phys.* **B497** (1997) 611.
- [6] S.-B. Liao and J. Polonyi, *Ann. Phys.* **222** (1993) 122 and *Phys. Rev.* **D51** (1995) 4474.
- [7] A. Patkos, P. Petreczky and J. Polonyi, *Ann. Phys.* **247** (1996) 78.
- [8] T. Roos, *Phys. Rev.* **D54** (1996) 2944.
- [9] J. D. Shafer and J. R. Shepard, *Phys. Rev.* **D55** (1997) 4990.
- [10] F.J. Wegner and A. Houghton, *Phys. Rev* **A8** (1972) 401.
- [11] see, for example, J. Polchinski, *Nucl. Phys.* **B231** (1984) 269;
A. Hasenfratz and P. Hasenfratz, *ibid.* **B270** (1986) 687.
- [12] P. Ginsparg, *Nucl. Phys.* **B170** (1980) 388.
- [13] R. Guida and J. Zinn-Justin, *Nucl. Phys.* **B489** (1997) 626.
- [14] T. R. Morris, *Int. J. Mod. Phys.* **A9** (1994) 2411; *Phys.Lett.* **B334** (1994) 355 and **B329** (1994) 241.
- [15] see, for example, C. M. Fraser, *Z. Phys.* **C28** (1985) 101;
A. Bonanno and D. Zappala, hep-th/9712038.
- [16] J. Alexandre, V. Branchina and J. Polonyi, hep-th/9709060 and hep-th/9712147.
- [17] S.-B. Liao, *Phys. Rev.* **D53** (1996) 2020, and *ibid.* **D56** (1997) 5008.
- [18] see, for example, M. Bonini, M. D’Attanasio and G. Marchesini, *Nucl. Phys.* **B437** (1995) 163 and **B409** (1993) 441;
M. Reuter and C. Wetterich, *ibid.* **B417** (1994) 181;
J. Comellas and A. Travesset, *ibid.* **B498** (1997) 539.
- [19] H. Matsumoto, Y. Nakano and H. Umezawa, *Phys. Rev.* **D29** (1984) 1116.
- [20] D. O’Connor and C. R. Stephens, *Int. J. Mod. Phys.* **A9** (1994) 2805.
- [21] J. Zinn-Justin, *Quantum Field Theory and Critical Phenomena*, (Clarendon, Oxford, 1989).
- [22] J. F. Nicoll, T. S. Chang and H. E. Stanley, *Phys. Rev. Lett.* **32** (1974) 1446, **33** (1974) 540; *Phys. Rev.* **A13** (1976) 1251.
- [23] H. A. Weldon, *J. Math. Phys.* **23** (1982) 1852.
- [24] L. Dolan and R. Jackiw, *Phys. Rev.* **D9** (1974) 3320.

FIGURE CAPTIONS

- Figure 1. Schematic diagram of blocking Method 1.
- Figure 2. Schematic diagram of blocking Method 2. The thickness of the RG shell in the n -axis is zero for $\Delta k \rightarrow 0$ (exaggerated here), but a Matsubara mode is eliminated after \mathcal{N} continuous iterations where $[\mathcal{N}\beta\Delta k/2\pi] = 1$.
- Figure 3. Schematic diagram of blocking Method 3.
- Figure 4. Plot of $g^{(3)}(\bar{\beta})$ for Method 3.
- Figure 5. Schematic diagram of blocking Method 4.
- Figure 6. Zero-temperature RG flow using Methods 1 and 3. The figure shows that as long as the correction to the UV cutoff is taken into account both methods give the same renormalized couplings at $T = 0$.
- Figure 7. Dependence of $\mu_{\beta,k}^2$ on δ . using Method 3.
- Figure 8. Temperature dependence of $g^{(2m)}$ in symmetric phase for $m = 1, \dots, 6$. The solid, dotted, dashed lines, and dot-dashed lines are for Methods 1, 2, 3, and 4 respectively.
- Figure 9. Comparison of $\lambda_{\beta,k}$ with different normalization conditions.

TABLE

- Table 1. Critical exponents and the effective coupling constant as a function of the level of polynomial truncation. Results for all four smearing functions are the same within the numerical accuracy. Errors reported here are due to numerics only and not that resulting from the polynomial truncation of the potential.